Lid-Driven Square Cavity Flow: A Benchmark Solution With an 8192 × 8192 Grid

Carlos Henrique Marchi
Laboratory of Numerical Experimentation (LENA),
Department of Mechanical Engineering (DEMEC),
Federal University of Paraná (UFPR),
Caixa Postal 19040,
Curitiba, PR 81531-980, Brazil
e-mail: chmcfd@gmail.com

Cosmo Damião Santiago
Federal University of Technology—Paraná (UTFPR),
Rua Marcílio Dias, 635 - Jardim Paraíso,
CEP 86812-460, Apucarana, PR, Brazil
e-mail: cosmo@utfpr.edu.br

Carlos Alberto Rezende de Carvalho, Jr.
Post-Graduate Program in Numerical Methods in Engineering (PPGMNE),
Federal University of Paraná (UFPR),
Curitiba, PR 81531-980, Brazil
e-mail: carloscarvalhoj@gmail.com

The incompressible steady-state fluid flow inside a lid-driven square cavity was simulated using the mass conservation and Navier–Stokes equations. This system of equations is solved for Reynolds numbers of up to 10,000 to the accuracy of the computational machine round-off error. The computational model used was the second-order accurate finite volume (FV) method. A stable solution is obtained using the iterative multigrid methodology with 8192 × 8192 volumes, while degree-10 interpolation and Richardson extrapolation were used to reduce the discretization error. The solution vector comprised five entries of velocities, pressure, and location. For comparison purposes, 65 different variables of interest were chosen, such as velocity profile, its extremum values and location, and extremum values and location of the stream function. The discretization error for each variable of interest was estimated using two types of estimators and their apparent order of accuracy. The variations of the 11 selected variables are shown across 38 Reynolds number values between 0.0001 and 10,000. In this study, we provide a more accurate determination of the Reynolds number value at which the upper secondary vortex appears. The results of this study were compared with those of several other studies in the literature. The current solution methodology was observed to produce the most accurate solution till date for a wide range of Reynolds numbers. [DOI: 10.1115/1.4052149]

1 Introduction

The laminar flow inside a square cavity caused by its movable lid was addressed in this study. A schematic of the problem proposed by Kawaguti in 1961 [1] is shown in Fig. 1. In addition, in Table 1, several other works [2–24] are cited that addressed the same problem using formulations such as stream function–vorticity (ψ–ω), the lattice Boltzmann equation (LBE), and Navier–Stokes equations (u, v, p). These studies used the finite difference (FD) method, finite volume (FV) method, finite element (FE) method, lattice Boltzmann (LB), spectral method (Spectral), smoothed particle hydrodynamics (SPH), wavelet-homotopy analysis method (wHAM), smoothed-profile method (SPM), and Chebyshev-collocation method (CCM). The grid resolutions ranged from 11 × 11 to 2048 × 2048, and the orders of accuracy (p_o) were mostly 1 and 2 but also 3, 5, 6, 7, 8, 10, and 160. The Reynolds number (Re) ranged from 0 to 50,000. The reviews of Shankar and Deshpande [25] and Kuhlmann and Romanò [26] cite several other works on the same problem, as well as on its three-dimensional version, i.e., the cubic cavity. Important information on various aspects of the cavity problem can be obtained in Refs. [27–29].

According to Ref. [13], there are two types of cavity problems: the first one, solved in the present work, is also known as "singular driven cavity" because there are two discontinuities in the boundary conditions of u (horizontal component of the velocity vector) in the corners of the lid, shown in Fig. 1: 0 on the walls and 1 on the lid. In Ref. [16], it is commented that due to these discontinuities, depending on the type of variable of interest, its value may not converge with the grid refinement; in the present work, all variables have a convergent value with the refinement of the grid. The second type of cavity problem is known as "regularized driven cavity," which has no discontinuities and is not addressed in this work.

The main objective of our study is to obtain the most accurate results for the lid-driven square cavity problem. This can be achieved by using the finest grid ever employed to solve the problem, as well as a recent technique to reduce the discretization error of variables with extremes and their coordinates, Richardson extrapolation to reduce the discretization error, verification of the order of accuracy, and using the iterative process until the machine round-off error is reached. The problem is solved by using the primitive variable formulation with the FV method, scheme of second-order accuracy, multigrid, double precision in calculations, and an 8192 × 8192 grid. This grid is approximately 1000 times larger than the largest grid used by Ghia et al. [6] (257 × 257), 16 times larger than the largest grid (2048 × 2048) already used in this problem by Bruneau and Saad [15] and Marchi et al. [20] with up to Re = 5000, and 64 times larger than the largest grid (1025 × 1025) already used in this problem by Erturk [17] for Re = 7500 and 10,000.

For each value of the Reynolds number equal to 1, 10, 100, 400, 1000, 3200, 5000, 7500, and 10,000, the results of 65 variables of interest are presented involving velocity profiles, their minimum and maximum values as well as their coordinates, and the minimum value of the stream function and its coordinates. This is probably the largest number of variables of interest presented for this problem. In addition, we present the estimated discretization error for each variable of interest according to two types of estimators and verify its order of accuracy, which are information that are rarely presented even in benchmarks.

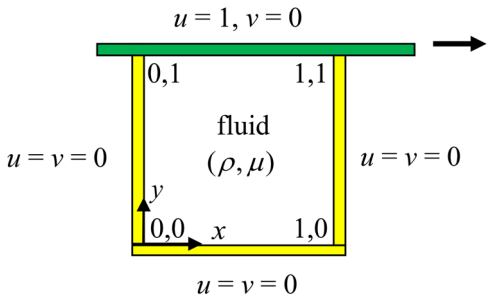

Fig. 1 Classical problem of the lid-driven square cavity flow

Manuscript received March 15, 2021; final manuscript received August 10, 2021; published online September 14, 2021. Assoc. Editor: Brian Freno.

Table 1 Some works that addressed the same problem

Reference	Formulation	Method	Grid	p_o	Re
[1]	ψ–ω	FD	11×11	2	0–64
[2]	ψ–ω	FD	51×51	2	0–700
[3]	ψ–ω	FD	128×128	2	100–1000
[4]	ψ–ω	FD	51×51	1	100–50,000
[5]	ψ–ω	FD	151×151	2	1000–10,000
[6]	ψ–ω	FD	257×257	2	100–10,000
[7]	ψ–ω	FD	180×180	2	1–10,000
[8]	u, v, p	FD	321×321	1	100–5000
[9]	ψ–ω	FD	129×129	10	100–3200
[10]	LBE	LB	256×256	1	100–7500
[11]	u, v, p	FV	1024×1024	2	100–1000
[12]	ψ–ω	FE	257×257	8	0.0001–12,500
[13]	u, v, p	Spectral	161×161	160	0–1000
[14]	ψ–ω	FD	601×601	2	1000–21,000
[15]	u, v, p	FD	2048×2048	2	1000–5000
[16]	u, v, p	FV	1024×1024	2	0.01–1000
[17]	ψ–ω	FD	1025×1025	2	1000–20,000
[18]	u, v, p	FD	257×257	3	1000–7500
[19]	u, v, p	SPH	Free	2	100–3200
[20]	u, v, p	FV	2048×2048	2	1000
[21]	u, v, p	FV	1301×1301	2	100–5000
[22]	ψ–ω	wHAM	64×64	6	0.01–1000
[23]	u, v, p	SPM	50×50	7	1000
[24]	u, v, p	CCM	128×128	5	1000
This work	u, v, p	FV	8192×8192	2	0.0001–10,000

The variation of the 11 selected variables in 38 values of Reynolds numbers between 0.0001 and 10,000 is shown. We herein show that the behavior of some variables is not monotonic with the Reynolds number, a point that is yet to be described in the literature but not with the grid resolution used herein. The results of this work are compared with several other studies in the literature, with an estimate of the discretization error whenever possible, considering the grid and order of accuracy of those studies. Finally, the Reynolds number at which the upper secondary vortex appears is determined more accurately, which was estimated to be 1200 by Benjamin and Denny [5] and 1500 by Vanka [8].

Given that the problem has no known analytical solution, highly accurate numerical results are important because (a) they can be used to evaluate the performance of existing or new discretization error estimators in realistic problems, i.e., problems that are not simulated or whose solution is arbitrarily proposed; (b) they can correctly show physical trends and behavior of variables; for example, the results of Refs. [5], [9–11], [19], [21], and [22] show that the minimum value of the stream function always decreases with an increase in the Reynolds number; however, the findings of Refs. [1], [2], [4], [6–8], [12], [14], [17], and [18] indicate a different behavior; and (c) they can be used to evaluate the performance of new numerical methods, new formulations, new approaches, and verification [30] of the results of new computational codes, among others.

2 Mathematical Model

The mathematical model of the problem comprises the laws of conservation of mass and conservation of momentum (the Navier–Stokes equations). The simplifications considered for the problem are the steady-state, two-dimensional laminar flow, constant density (ρ), and viscosity (μ) of the fluid. Thus, the resulting mathematical model in Cartesian coordinates in the x- and y-directions is

$$\frac{\partial u}{\partial x} + \frac{\partial v}{\partial y} = 0 \tag{1}$$

$$\frac{\partial (u^2)}{\partial x} + \frac{\partial (uv)}{\partial y} = \frac{1}{\mathrm{Re}}\left(\frac{\partial^2 u}{\partial x^2} + \frac{\partial^2 u}{\partial y^2}\right) - \frac{\partial p}{\partial x} \tag{2}$$

$$\frac{\partial (uv)}{\partial x} + \frac{\partial (v^2)}{\partial y} = \frac{1}{\mathrm{Re}}\left(\frac{\partial^2 v}{\partial x^2} + \frac{\partial^2 v}{\partial y^2}\right) - \frac{\partial p}{\partial y} \tag{3}$$

where

$$\mathrm{Re} = \frac{\rho U L}{\mu} \tag{4}$$

and Re is the Reynolds number, u and v denote the components of the velocity vector in the x- and y-directions, respectively, p is the pressure, and U and L are, respectively, velocity and length characteristic of the problem with unit values, that is, $U = 1$ m/s and $L = 1$ m. The domain is a square with the origin of the system of coordinates, as shown in Fig. 1, and a dimension of $1 \times 1\,\mathrm{m}^2$. Moreover, $\rho = 1\,\mathrm{kg/m}^3$.

The 65 variables of interest of the problem are (i) profile of u at $x = 1/2$ at 28 selected points of y; (ii) profile of v at $y = 1/2$ at 28 selected points of x; (iii) the minimum value ($u_{\min}$) of profile of u at $x = 1/2$ and its respective y coordinate: $y(u_{\min})$; (iv) the minimum ($v_{\min}$) and the maximum ($v_{\max}$) values of profile of v at $y = 1/2$ and their respective x coordinates, i.e., $x(v_{\min})$ and $x(v_{\max})$; and (v) the minimum value of the stream function ($\psi_{\min}$) and its coordinates x and y, that is, $x(\psi_{\min})$ and $y(\psi_{\min})$.

3 Numerical Model

The computational code used here was adapted from Ref. [31] (see Appendix A.1), written in FORTRAN 77, and available on the Internet. The code was migrated to FORTRAN 95, using an Intel FORTRAN Composer XE 2013 double-precision compiler, and extended to obtain the results according to the focus of this study. The part added to the source code includes subroutines to obtain the necessary points to apply interpolations, as well as the minimum and/or maximum value (base point) in the field of solutions, its neighbors in spatial directions, and their respective coordinates. The iterative process is repeated in the finest grid until the machine round-off error is reached. This is verified by monitoring the maximum L_1-norm along the iterations of the residual (R) of the three solved systems of equations. The calculations were performed on a Dell OptiPlex 7050 desktop computer equipped with an Intel Core i7-6700 vPro 3.40-GHz processor, Windows 10 Pro operating system, and 32-GB RAM 2.4-GHz DIMM.

The mathematical model described by Eqs. (1)–(3) is solved using the following tools: (1) the FV method; (2) central difference scheme for diffusive and pressure terms; (3) central difference scheme with deferred correction [31,32] on the upstream difference scheme for advective terms; (4) Eqs. (1)–(3) are sequentially solved using the strongly implicit procedure method [33]; (5) the semi-implicit linked equations method [34] is used to treat pressure–velocity coupling; and (6) Dirichlet boundary conditions are used for u and v, Fig. 1: no-slip boundary condition applies, i.e., the velocity of the fluid is equal to the wall velocity, which is null except on the lid that has a constant and unitary speed. For pressure or pressure correction, linear extrapolation was applied from the interior to the boundary [31]. The boundary conditions on all grid levels on the multigrid are treated in the same manner as those in any single-grid algorithm. (7) The underrelaxation factors are set to 0.8 for the velocity components and 0.2 for the pressure, respectively, on all grid levels. (8) Solutions were obtained with approximations of second-order accuracy, and (9) uniform grids were used.

To obtain numerical solutions on the finest grid at a low computational cost, the multigrid method with V-cycle and full approximation scheme is applied for outer iterations with the collocated variable arrangement in uniform grids. The same restriction and prolongation operators for the transfer of information between the various grids were used for all variables: (a) in the prolongation, bilinear interpolation; (b) in the restriction, the coarse grid control volume (CV) comprises four fine-grid CVs. The residuals are thus

added to the fine-grid CVs, and the initial mass flux at the coarse CV faces is the sum of the mass fluxes at the fine CV faces. There is no need to transfer pressure-related information between the various grids, e.g., pressure corrections, see Ref. [31]. Emphasizing that the computational effort is proportional to the size of the problem when the solver is associated with the multigrid method. The multigrid method was used herein because it enabled us to obtain solutions without iteration errors in very fine grids in a short CPU time. The efficiency of calculating steady incompressible flows using implicit methods based on the semi-implicit linked equations algorithm and on collocated grids with Rhie–Chow correction [35], using the multigrid method for outer iterations was demonstrated in two test cases by Ferziger et al. [31]. The details of the multigrid methods are available in Ref. [36].

The variables of interest are calculated in postprocessing, as follows:

- The numerical solution of the profile of u at $x = 1/2$ is obtained from u stored at the east face of the volumes for each desired y coordinate. This u at each east face of the CV is one of the collocated arrangements of the variables discussed in Ref. [31]. This is necessary because the number of volumes used in each coordinate direction is even so that no CV center coincides with the line $x = 1/2$. The arithmetic mean of two values of u stored at the center of the faces is determined by $x = 1/2$, one u above and one below each y coordinate desired for u.
- The numerical solution of the profile of v at $y = 1/2$ is analogously obtained to the profile of u, through of v stored at the north face of the volumes for each desired x coordinate. The arithmetic mean of the two values of v stored at the center of the faces is determined by $y = 1/2$, one v on the left and one on the right of each x coordinate desired for v.
- $u_{\min}$ is the minimum value of the solution of u stored at the east faces of all CVs of the grid with $x = 1/2$, and its y coordinate is the one at the center of the east face of the volume corresponding to $u_{\min}$.
- $v_{\min}$ and $v_{\max}$ are the minimum and maximum values of the solution of v stored at the north face of all CVs of the grid with $y = 1/2$, and their x coordinates are the ones at the center of the north face of the volumes corresponding to $v_{\min}$ and $v_{\max}$.
- The numerical solution of the stream function field (ψ) is computed in postprocessing by tallying up volume fluxes through faces starting from the lower wall, at $y = 0$. The value at the next vertex is computed by adding the volume flux through the face connecting the two vertices. The vertical lines coincide with the x coordinates of the faces of each CV. The minimum value of the stream function ($\psi_{\min}$) is obtained directly from the ψ field, as well as its respective x and y coordinates.

All variables obtained in the above-described manner are generically denoted by T_h.

To reduce the discretization error of $u_{\min}$, $v_{\min}$, $v_{\max}$, and $\psi_{\min}$, we used the following strategy proposed in Ref. [20]. Taking the variable $u_{\min}$ as an example, a degree-10 polynomial was fitted around the coordinate $y(u_{\min})$ of the grid, with ten other values of u in neighbors of y coordinates, with five points on each side of $y(u_{\min})$, totaling 11 points of u and y of the grid. Subsequently, the y coordinate and the minimum u value of the polynomial were determined by interpolation. The same procedure was applied to the variables $v_{\min}$ and $v_{\max}$ and their respective coordinates. In the case of the variable $\psi_{\min}$, 11 polynomials of degree 10 were adjusted in both directions, totaling 121 points. Then, the x and y coordinates corresponding to the minimum ψ value of the two-dimensional surface generated by the polynomials were calculated by two-dimensional interpolation. All variables obtained in this manner, that is, through interpolation, are generically denoted by T_p.

4 Results

To verify the convergence of the solutions with grid refinement, as well as the apparent order (p_U) of the discretization error, the problem for each Reynolds number was solved in grids of 2×2, 4×4, 8×8, 16×16, 32×32, 64×64, and so on up to 8192×8192, that is, with a grid refinement ratio (r) equal to 2, involving up to 13 grids. The RAM required to solve the problem in the finest grid was 21.5 GB.

The number of iterations performed (Itmax) for each Reynolds number, the number of iterations required to reach the machine round-off error (Itπ), the CPU time (t-cpu) required for Itmax in days (d), hours (h), and minutes (min), and the dimensionless residual of each equation solved in Itmax (R_u, R_v, and R_p) are shown in Table 2. $\Delta\phi$-max is the maximum amplitude of the oscillation of the result in the last 50 iterations in relation to the result obtained in Itmax for five control variables. In general, Itπ, t-cpu, R_u, R_v, and R_p increase as the Reynolds number increases, but R_p is not very sensitive. No attempt was made to optimize the multigrid parameters to reduce t-cpu. $\Delta\phi$-max is practically constant because it is virtually insensitive to the Reynolds number. The values of $\Delta\phi$-max indicate that the level of iteration and rounding errors in the solutions of the variables of interest are less than 1×10^{-13}; hence, the numerical error will almost solely comprise the discretization error.

The curves of the L_1-norm of the dimensionless residuals of the three systems of algebraic equations solved as a function of the number of iterations performed for $\mathrm{Re} = 10{,}000$ and 8192×8192 volumes are shown in Fig. 2. After 10,000 iterations, the residuals have stabilized, indicating that the machine round-off error has been reached, thereby reducing the iteration error to the minimum possible. In all the grids and for all Reynolds numbers, the machine round-off error was reached for double precision in the calculations, as shown in Table 2 for the grid of 8192×8192 volumes. For each grid and Reynolds number, Itmax was determined by trial and error until the machine round-off error level was reached with It$\pi <$ Itmax, as shown in Fig. 2.

To estimate the discretization error, the grid convergence index (GCI) estimator [37] was used because it is widely reported in the literature and adopted in the ASME standard [30], thereby serving

Table 2 Convergence properties, 8192 × 8192 grid

Re	Itmax	Itπ	t-cpu	R_u	R_v	R_p	$\Delta\phi$-max
1	150	78	2 h 23 min	4.1×10^{-9}	3.4×10^{-9}	1.6×10^{-13}	3.6×10^{-14}
10	150	76	2 h 16 min	3.8×10^{-10}	3.1×10^{-10}	1.5×10^{-13}	9.8×10^{-14}
100	200	75	3 h 10 min	4.0×10^{-11}	3.5×10^{-11}	1.7×10^{-13}	5.5×10^{-14}
400	150	75	2 h 22 min	1.1×10^{-11}	1.1×10^{-11}	2.1×10^{-13}	6.9×10^{-14}
1000	200	85	3 h 21 min	5.3×10^{-12}	5.3×10^{-12}	2.3×10^{-13}	3.5×10^{-14}
3200	700	320	12 h 11 min	1.9×10^{-12}	1.9×10^{-12}	2.5×10^{-13}	2.8×10^{-14}
5000	1000	580	23 h 17 min	1.2×10^{-12}	1.2×10^{-12}	2.5×10^{-13}	1.3×10^{-14}
7500	4000	2800	2 d 17 h 52 min	8.4×10^{-13}	8.3×10^{-13}	2.5×10^{-13}	1.7×10^{-14}
10,000	12,000	10,000	5 d 09 h 50 min	6.7×10^{-13}	6.6×10^{-13}	2.6×10^{-13}	4.5×10^{-14}

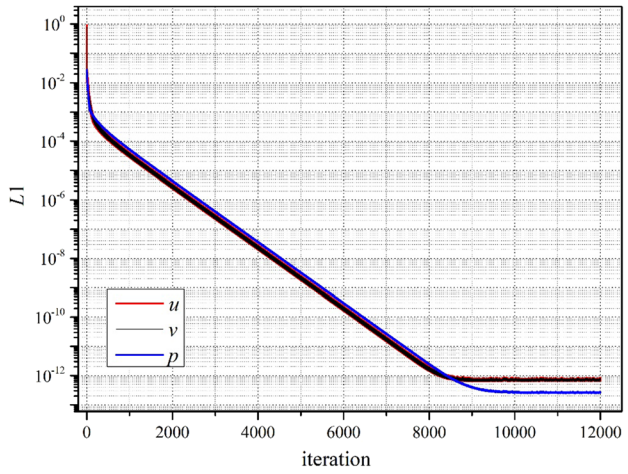

Fig. 2 Residuals of equations for Re = 10,000 and 8192 × 8192 grid

as a reference or standard estimator in the literature. In this study, the GCI was applied as follows:

$$\mathrm{GCI} = F_S \frac{|T_1 - T_2|}{(r^p - 1)} \tag{5}$$

where T_1 and T_2 represent numerical solutions obtained based on the 8192×8192 and 4096×4096 grids, respectively, $r = 2$ (grid refinement ratio), $F_S = 1.25$ (safety factor for 95% confidence), $p = \mathrm{Min}(p_o, p_U)$ for $p_U > 0$, where p_o is the order of accuracy of the numerical method used, and the equivalent apparent order (p_U) of the discretization error is given by

$$p_U = \frac{\log\left|\dfrac{T_2 - T_3}{T_1 - T_2}\right|}{\log(r)} \tag{6}$$

where T_3 is the numerical solution obtained based on the 2048×2048 grid.

Owing to the excellent results in Ref. [38], the convergent solution (T_c) is used here to reduce the discretization error by means of simple postprocessing using the numerical solutions T_h or T_p in three grids. The convergent solution (T_c) is calculated as follows [39]:

$$T_c = \frac{T_\infty(p_o) + T_\infty(p_U)}{2} \tag{7}$$

where $T_\infty(p_o)$ and $T_\infty(p_U)$ are determined by the Richardson extrapolation, that is,

$$T_\infty(p_o) = T_1 + \frac{(T_1 - T_2)}{(r^{p_o} - 1)} \tag{8}$$

$$T_\infty(p_U) = T_1 + \frac{(T_1 - T_2)}{(r^{p_U} - 1)} \tag{9}$$

for $p_U > 0$. The discretization error (U_c) of the solution T_c is estimated as follows [39]:

$$U_c = \frac{|T_\infty(p_o) - T_\infty(p_U)|}{2} \tag{10}$$

Next, the detailed results for each of the nine Reynolds number values are described in Secs. 4.1–4.9. The discussions on these results are presented in Sec. 4.10.

4.1 Re = 1. The results for Re = 1 of the variables with extremes based on the 8192×8192 grid are shown in Table 3, where T represents each variable of interest, p_U is the equivalent apparent order of the discretization error, and T_p represents the solution of each variable of interest, as described in Sec. 3, GCI [37] is an estimate of the discretization error, T_c is the convergent solution, and U_c is its estimate of the discretization error [39], and $|T_c\text{-}[Z]|$ is the absolute value of the difference between the solution T_c and the solution of the aforementioned reference Z. The GCI and U_c values, which are shown in parentheses, refer to the last two digits of the T_p and T_c values. For example, the value $-2.07754053 \times 10^{-1}(43)$ means that $\mathrm{GCI} = 4.3 \times 10^{-8}$, while the value $-2.0775408695 \times 10^{-1}(12)$ means that $U_c = 1.2 \times 10^{-10}$.

The results for Re = 1 for the velocity profiles as well as the value of the equivalent apparent order (p_U) calculated using Eq. (6) are shown in Tables 4 and 5. The x and y coordinates used here are the same as those employed in Refs. [6] and [16]; their values are exact, i.e., there is no rounding. In these tables, T_h represents the solution for each variable of interest, as described in Sec. 3.

The comparisons of $\psi_{\min}$ with that of other author for Re = 1 are shown in Table 6. The grid column indicates the number of grid nodes in each coordinated direction, p_o is the order of accuracy of the numerical solution according to each author, and RE is the number of repeated Richardson extrapolations as per Ref. [20]. In this table and in the following ones of the same type, the column denoted by U represents an estimate of the discretization error, which may have been obtained through one of the following ways: A = the estimate is from the cited work; B = the estimate is made via the GCI using Eq. (5), $p = p_o$ and $Fs = 3$ using results in two grids of the cited work; C = the estimate is calculated using the GCI according to Eq. (5) and its explanatory text, using results in three grids of the cited work; O = the estimate is calculated differently by the authors of the cited work; or M = the estimate is calculated herein using Eq. (10). The column denoted by D represents the absolute value of the difference between each solution presented and the reference solution (ref), which is always T_c based on the 8192×8192 grid, and this represents the best result of this study for each Reynolds number. Finally, the column identified by R represents the ratio between U and D; if $R \geq 1$, it means that U is reliable, i.e., U is greater than or equal to D. The closer R is to the unit, the more accurate is the estimated error of

Table 3 Results of the variables with extremes, Re = 1, 8192 × 8192 grid

T	p_U	T_p(GCI)	$T_c(U_c)$	$\lvert T_c\text{-}[7]\rvert$	$\lvert T_c\text{-}[12]\rvert$
$u_{\min}$	1.992	$-2.07754053 \times 10^{-1}$ (43)	$-2.0775408695 \times 10^{-1}$ (12)		
$y(u_{\min})$	2.010	$5.35913245 \times 10^{-1}$ (32)	$5.3591326968 \times 10^{-1}$ (12)		
$v_{\min}$	1.974	$-1.84827306 \times 10^{-1}$ (18)	$-1.8482732023 \times 10^{-1}$ (17)		
$x(v_{\min})$	2.005	$7.90795220 \times 10^{-1}$ (36)	$7.90795191718 \times 10^{-1}$ (70)		
$v_{\max}$	1.976	$1.84067775 \times 10^{-1}$ (18)	$1.8406778975 \times 10^{-1}$ (16)		
$x(v_{\max})$	2.005	$2.09765245 \times 10^{-1}$ (35)	$2.09765272832 \times 10^{-1}$ (62)		
$\psi_{\min}$	1.987	$-1.00076622 \times 10^{-1}$ (11)	$-1.00076630770 \times 10^{-1}$ (53)	1.7×10^{-5}	2.7×10^{-5}
$x(\psi_{\min})$	2.428	$5.01671789217 \times 10^{-1}$ (61)	$5.016717891756 \times 10^{-1}$ (77)	1.7×10^{-3}	
$y(\psi_{\min})$	1.923	$7.650244469 \times 10^{-1}$ (30)	$7.65024444599 \times 10^{-1}$ (83)	1.6×10^{-3}	

Table 4 Profile of u at $x = 1/2$, Re = 1, and 8192 × 8192 grid

$u(y)$	p_U	T_h(GCI)	$T_c(U_c)$
$u(0.0546875)$	2.062	$-3.42187829 \times 10^{-2}$ (15)	$-3.4218781703 \times 10^{-2}$ (33)
$u(0.0625)$	2.058	$-3.85276912 \times 10^{-2}$ (17)	$-3.8527689832 \times 10^{-2}$ (36)
$u(0.0703125)$	2.056	$-4.27228319 \times 10^{-2}$ (20)	$-4.2722830393 \times 10^{-2}$ (39)
$u(0.1015625)$	2.053	$-5.85353574 \times 10^{-2}$ (27)	$-5.8535355228 \times 10^{-2}$ (52)
$u(0.125)$	2.055	$-6.95848138 \times 10^{-2}$ (31)	$-6.9584811431 \times 10^{-2}$ (61)
$u(0.171875)$	2.077	$-9.02885205 \times 10^{-2}$ (28)	$-9.0288518300 \times 10^{-2}$ (75)
$u(0.1875)$	2.095	$-9.69074813 \times 10^{-2}$ (24)	$-9.6907479469 \times 10^{-2}$ (79)
$u(0.25)$	1.696	$-1.225968059 \times 10^{-1}$ (14)	$-1.2259680687 \times 10^{-1}$ (14)
$u(0.28125)$	1.917	$-1.351298538 \times 10^{-1}$ (42)	$-1.3512985708 \times 10^{-1}$ (13)
$u(0.3125)$	1.955	$-1.474634520 \times 10^{-1}$ (79)	$-1.4746345823 \times 10^{-1}$ (13)
$u(0.375)$	1.978	$-1.71069031 \times 10^{-1}$ (18)	$-1.7106904454 \times 10^{-1}$ (14)
$u(0.4375)$	1.987	$-1.91537294 \times 10^{-1}$ (30)	$-1.9153731861 \times 10^{-1}$ (14)
$u(0.453125)$	1.988	$-1.95779334 \times 10^{-1}$ (34)	$-1.9577936081 \times 10^{-1}$ (14)
$u(0.5)$	1.992	$-2.05191395 \times 10^{-1}$ (45)	$-2.0519143075 \times 10^{-1}$ (14)
$u(0.5625)$	1.995	$-2.06086144 \times 10^{-1}$ (59)	$-2.0608619123 \times 10^{-1}$ (10)
$u(0.6171875)$	1.998	$-1.89675415 \times 10^{-1}$ (67)	$-1.89675468515 \times 10^{-1}$ (54)
$u(0.625)$	1.998	$-1.85574552 \times 10^{-1}$ (68)	$-1.85574605784 \times 10^{-1}$ (45)
$u(0.6875)$	2.002	$-1.32200974 \times 10^{-1}$ (66)	$-1.32201026510 \times 10^{-1}$ (43)
$u(0.734375)$	2.006	$-6.2493180 \times 10^{-2}$ (55)	$-6.249322374 \times 10^{-2}$ (12)
$u(0.75)$	2.008	$-3.2438028 \times 10^{-2}$ (50)	$-3.243806817 \times 10^{-2}$ (15)
$u(0.8125)$	2.032	$1.27053510 \times 10^{-1}$ (21)	$1.2705349382 \times 10^{-1}$ (24)
$u(0.8515625)$	2.539	$2.613899556 \times 10^{-1}$ (12)	$2.6138995484 \times 10^{-1}$ (18)
$u(0.875)$	1.904	$3.552202965 \times 10^{-1}$ (93)	$3.5522030359 \times 10^{-1}$ (32)
$u(0.9375)$	1.967	$6.51169848 \times 10^{-1}$ (19)	$6.5116986295 \times 10^{-1}$ (23)
$u(0.953125)$	1.969	$7.34328876 \times 10^{-1}$ (17)	$7.3432888937 \times 10^{-1}$ (19)
$u(0.9609375)$	1.969	$7.77057430 \times 10^{-1}$ (15)	$7.7705744160 \times 10^{-1}$ (17)
$u(0.96875)$	1.969	$8.20483009 \times 10^{-1}$ (13)	$8.2048301878 \times 10^{-1}$ (14)
$u(0.9765625)$	1.968	$8.64549935 \times 10^{-1}$ (10)	$8.6454994285 \times 10^{-1}$ (12)

Table 5 Profile of v at $y = 1/2$, Re = 1, and 8192 × 8192 grid

$v(x)$	p_U	T_h(GCI)	$T_c(U_c)$
$v(0.0625)$	1.772	$9.44033586 \times 10^{-2}$ (17)	$9.440335979 \times 10^{-2}$ (13)
$v(0.0703125)$	1.865	$1.039698337 \times 10^{-1}$ (28)	$1.0396983582 \times 10^{-1}$ (13)
$v(0.078125)$	1.905	$1.129986521 \times 10^{-1}$ (41)	$1.1299865524 \times 10^{-1}$ (14)
$v(0.09375)$	1.942	$1.294175347 \times 10^{-1}$ (72)	$1.2941754029 \times 10^{-1}$ (15)
$v(0.125)$	1.968	$1.55623178 \times 10^{-1}$ (15)	$1.5562318964 \times 10^{-1}$ (17)
$v(0.15625)$	1.979	$1.73084719 \times 10^{-1}$ (23)	$1.7308473739 \times 10^{-1}$ (18)
$v(0.1875)$	1.985	$1.82236343 \times 10^{-1}$ (31)	$1.8223636723 \times 10^{-1}$ (17)
$v(0.2265625)$	1.989	$1.83079577 \times 10^{-1}$ (38)	$1.8307960726 \times 10^{-1}$ (15)
$v(0.234375)$	1.990	$1.81970687 \times 10^{-1}$ (39)	$1.8197071815 \times 10^{-1}$ (15)
$v(0.25)$	1.991	$1.78592666 \times 10^{-1}$ (40)	$1.7859269767 \times 10^{-1}$ (14)
$v(0.3125)$	1.993	$1.51806580 \times 10^{-1}$ (40)	$1.51806611313 \times 10^{-1}$ (98)
$v(0.375)$	1.995	$1.09232513 \times 10^{-1}$ (31)	$1.09232537946 \times 10^{-1}$ (60)
$v(0.4375)$	1.995	5.7162281×10^{-2} (16)	$5.7162294542 \times 10^{-2}$ (30)
$v(0.5)$	2.037	6.3676365×10^{-4} (35)	$6.367633727 \times 10^{-4}$ (47)
$v(0.5625)$	1.997	$-5.6054827 \times 10^{-2}$ (17)	$-5.6054841073 \times 10^{-2}$ (21)
$v(0.625)$	1.995	$-1.08578875 \times 10^{-1}$ (32)	$-1.08578900245 \times 10^{-1}$ (53)
$v(0.6875)$	1.994	$-1.51763392 \times 10^{-1}$ (40)	$-1.51763424616 \times 10^{-1}$ (95)
$v(0.75)$	1.991	$-1.79114891 \times 10^{-1}$ (41)	$-1.7911492335 \times 10^{-1}$ (14)
$v(0.8046875)$	1.985	$-1.84110842 \times 10^{-1}$ (32)	$-1.8411086739 \times 10^{-1}$ (17)
$v(0.8125)$	1.984	$-1.83060712 \times 10^{-1}$ (30)	$-1.8306073607 \times 10^{-1}$ (18)
$v(0.859375)$	1.972	$-1.66221563 \times 10^{-1}$ (18)	$-1.6622157771 \times 10^{-1}$ (18)
$v(0.875)$	1.964	$-1.56358749 \times 10^{-1}$ (14)	$-1.5635875990 \times 10^{-1}$ (18)
$v(0.90625)$	1.927	$-1.299791304 \times 10^{-1}$ (61)	$-1.2997913513 \times 10^{-1}$ (16)
$v(0.9375)$	1.101	$-9.47480769 \times 10^{-2}$ (12)	$-9.474807752 \times 10^{-2}$ (30)
$v(0.9453125)$	2.585	$-8.459775187 \times 10^{-2}$ (38)	$-8.4597751627 \times 10^{-2}$ (60)
$v(0.953125)$	2.220	$-7.393096419 \times 10^{-2}$ (99)	$-7.3930963466 \times 10^{-2}$ (72)
$v(0.9609375)$	2.136	$-6.27615351 \times 10^{-2}$ (14)	$-6.2761534099 \times 10^{-2}$ (65)
$v(0.96875)$	2.098	$-5.11053213 \times 10^{-2}$ (16)	$-5.1105320098 \times 10^{-2}$ (53)

U. The results in this table are presented sequentially, from top to bottom, from the highest to the lowest D.

4.2 Re = 10. The results for Re = 10 for the variables with extremes based on the 8192 × 8192 grid are shown in Table 7. The results for Re = 10 for the velocity profiles are displayed in Tables 8 and 9. Comparisons with other authors of $\psi_{\min}$ for Re = 10 are presented in Table 10.

4.3 Re = 100. The results for Re = 100 for the variables with extremes based on the 8192 × 8192 grid are shown in Table 11; in column $|T_c$-[13]|, the results of $\psi_{\min}$ and its coordinates are from Ref. [11]. The results for Re = 100 for the velocity profiles are

Table 6 Comparisons of ψ_{min}, Re = 1

Reference	Grid	p_o	RE	$-\psi_{min}$	U	D	R
[12]	5	6		0.10005		2.7×10^{-5}	
This work	2048	2		0.10007649		1.4×10^{-7}	
This work	4096	2		0.10007660	B: 1.0×10^{-7}	3.1×10^{-8}	3.3
This work	8192	2		0.100076622	C: 1.1×10^{-8}	8.7×10^{-9}	1.3
This work	8192	2	1	0.100076630770	M: 5.3×10^{-11}	**0 = ref**	

Note: The bold value indicates the best result of this work for ψ_{min}.

Table 7 Results of the variables with extremes, Re = 10, 8192 × 8192 grid

T	p_U	T_p(GCI)	$T_c(U_c)$	$\lvert T_c$-[16]$\rvert$	$\lvert T_c$-[22]$\rvert$	$\lvert T_c$-[2]$\rvert$
u_{min}	1.993	$-2.07576259 \times 10^{-1}$ (43)	$-2.0757629311 \times 10^{-1}$ (12)	2.07×10^{-7}	8.1×10^{-6}	
$y(u_{min})$	2.010	$5.34819809 \times 10^{-1}$ (31)	$5.3481983352 \times 10^{-1}$ (12)	1.50×10^{-4}	3.6×10^{-3}	
v_{min}	1.966	$-1.88505887 \times 10^{-1}$ (16)	$-1.8850589967 \times 10^{-1}$ (20)	3.00×10^{-7}	4.2×10^{-5}	
$x(v_{min})$	2.007	$7.93271321 \times 10^{-1}$ (42)	$7.9327128788 \times 10^{-1}$ (10)	1.89×10^{-4}	3.6×10^{-3}	
v_{max}	1.983	$1.80911518 \times 10^{-1}$ (21)	$1.8091153523 \times 10^{-1}$ (14)	1.65×10^{-7}	4.2×10^{-5}	
$x(v_{max})$	2.002	$2.12320423 \times 10^{-1}$ (29)	$2.12320446299 \times 10^{-1}$ (25)	7.96×10^{-5}	6.4×10^{-3}	
ψ_{min}	1.987	$-1.00112739 \times 10^{-1}$ (11)	$-1.00112747639 \times 10^{-1}$ (54)	4.52×10^{-7}	2.4×10^{-5}	2.1×10^{-4}
$x(\psi_{min})$	2.390	$5.1665734059 \times 10^{-1}$ (62)	$5.16657340161 \times 10^{-1}$ (73)	5.73×10^{-5}	1.0×10^{-3}	
$y(\psi_{min})$	1.927	$7.648154401 \times 10^{-1}$ (31)	$7.64815437696 \times 10^{-1}$ (82)	1.65×10^{-4}	8.1×10^{-4}	

Table 8 Profile of u at $x = 1/2$, Re = 10, and 8192 × 8192 grid

$u(y)$	p_U	T_h(GCI)	$T_c(U_c)$	$\lvert T_c$-[16]$\rvert$
$u(0.0546875)$	2.060	$-3.42314391 \times 10^{-2}$ (15)	$-3.4231437923 \times 10^{-2}$ (32)	
$u(0.0625)$	2.057	$-3.85425814 \times 10^{-2}$ (17)	$-3.8542580104 \times 10^{-2}$ (35)	1.0×10^{-10}
$u(0.0703125)$	2.055	$-4.27401071 \times 10^{-2}$ (19)	$-4.2740105626 \times 10^{-2}$ (38)	
$u(0.1015625)$	2.053	$-5.85638994 \times 10^{-2}$ (27)	$-5.8563897297 \times 10^{-2}$ (51)	
$u(0.125)$	2.055	$-6.96238585 \times 10^{-2}$ (30)	$-6.9623856199 \times 10^{-2}$ (59)	9.9×10^{-11}
$u(0.171875)$	2.078	$-9.03543739 \times 10^{-2}$ (27)	$-9.0354371827 \times 10^{-2}$ (74)	
$u(0.1875)$	2.099	$-9.69839640 \times 10^{-2}$ (22)	$-9.6983962262 \times 10^{-2}$ (77)	2.6×10^{-10}
$u(0.25)$	1.773	$-1.227219774 \times 10^{-1}$ (17)	$-1.2272197864 \times 10^{-1}$ (13)	4×10^{-10}
$u(0.28125)$	1.926	$-1.352802732 \times 10^{-1}$ (46)	$-1.3528027673 \times 10^{-1}$ (12)	
$u(0.3125)$	1.958	$-1.476361913 \times 10^{-1}$ (84)	$-1.4763619795 \times 10^{-1}$ (13)	1.1×10^{-9}
$u(0.375)$	1.979	$-1.71260741 \times 10^{-1}$ (18)	$-1.7126075568 \times 10^{-1}$ (14)	1.4×10^{-9}
$u(0.4375)$	1.988	$-1.91677017 \times 10^{-1}$ (31)	$-1.9167704142 \times 10^{-1}$ (14)	1.6×10^{-9}
$u(0.453125)$	1.989	$-1.95889491 \times 10^{-1}$ (35)	$-1.9588951895 \times 10^{-1}$ (14)	
$u(0.5)$	1.992	$-2.05164699 \times 10^{-1}$ (46)	$-2.0516473580 \times 10^{-1}$ (13)	2.2×10^{-9}
$u(0.5625)$	1.995	$-2.05770148 \times 10^{-1}$ (59)	$-2.0577019545 \times 10^{-1}$ (10)	2.6×10^{-9}
$u(0.6171875)$	1.998	$-1.89066549 \times 10^{-1}$ (67)	$-1.89066602072 \times 10^{-1}$ (51)	
$u(0.625)$	1.998	$-1.84928060 \times 10^{-1}$ (68)	$-1.84928113586 \times 10^{-1}$ (42)	2.5×10^{-9}
$u(0.6875)$	2.002	$-1.31389182 \times 10^{-1}$ (65)	$-1.31389234641 \times 10^{-1}$ (45)	7×10^{-10}
$u(0.734375)$	2.006	$-6.1822984 \times 10^{-2}$ (55)	$-6.182302725 \times 10^{-2}$ (12)	
$u(0.75)$	2.008	$-3.1879270 \times 10^{-2}$ (49)	$-3.187930907 \times 10^{-2}$ (15)	1.1×10^{-9}
$u(0.8125)$	2.032	$1.26912107 \times 10^{-1}$ (20)	$1.2691209151 \times 10^{-1}$ (24)	3.9×10^{-9}
$u(0.8515625)$	2.870	$2.6078424437 \times 10^{-1}$ (63)	$2.6078424400 \times 10^{-1}$ (13)	
$u(0.875)$	1.914	$3.544303526 \times 10^{-1}$ (99)	$3.5443036022 \times 10^{-1}$ (31)	3.8×10^{-9}
$u(0.9375)$	1.969	$6.50529274 \times 10^{-1}$ (20)	$6.5052928951 \times 10^{-1}$ (22)	2.5×10^{-9}
$u(0.953125)$	1.971	$7.33859160 \times 10^{-1}$ (18)	$7.3385917428 \times 10^{-1}$ (19)	
$u(0.9609375)$	1.971	$7.76681352 \times 10^{-1}$ (16)	$7.7668136403 \times 10^{-1}$ (17)	
$u(0.96875)$	1.971	$8.20200815 \times 10^{-1}$ (13)	$8.2020082572 \times 10^{-1}$ (14)	
$u(0.9765625)$	1.970	$8.64357325 \times 10^{-1}$ (11)	$8.6435733347 \times 10^{-1}$ (12)	

displayed in Tables 12 and 13. Comparisons with other authors of ψ_{min} for Re = 100 are presented in Table 14.

4.4 Re = 400. The results for Re = 400 for the variables with extremes based on the 8192 × 8192 grid are shown in Table 15. The results for Re = 400 for the velocity profiles are displayed in Tables 16 and 17. Comparisons with other authors of ψ_{min} for Re = 400 are presented in Table 18.

4.5 Re = 1000. The results for Re = 1000 for the variables with extremes based on the 8192 × 8192 grid are shown in Table 19; in column $\lvert T_c$-[24]$\rvert$, the results of ψ_{min} and its coordinates are from Ref. [23]. The results for Re = 1000 for the velocity profiles are displayed in Tables 20 and 21. Comparisons with other authors of ψ_{min} for Re = 1000 are presented in Table 22.

4.6 Re = 3200. The results for Re = 3200 for the variables with extremes based on the 8192 × 8192 grid are shown in Table 23; in column $\lvert T_c$-[19]$\rvert$, the results of ψ_{min} and its coordinates are from Ref. [21], while those in column $\lvert T_c$-[18]$\rvert$ are from Ref. [9]. The results for Re = 3200 for the velocity profiles are displayed in Tables 24 and 25. Comparisons with other authors of ψ_{min} for Re = 3200 are presented in Table 26.

4.7 Re = 5000. The results for Re = 5000 for the variables with extremes based on the 8192 × 8192 grid are shown in

Table 9 Profile of v at $y = 1/2$, Re = 10, and 8192 × 8192 grid

$v(x)$	p_U	T_h(GCI)	$T_c(U_c)$	$\lvert T_c$-[16]$\rvert$
$v(0.0625)$	1.960	$9.29701145 \times 10^{-2}$ (57)	$9.2970119008 \times 10^{-2}$ (84)	2×10^{-9}
$v(0.0703125)$	1.965	$1.023035926 \times 10^{-1}$ (71)	$1.02303598213 \times 10^{-1}$ (92)	
$v(0.078125)$	1.968	$1.111007471 \times 10^{-1}$ (86)	$1.11100753927 \times 10^{-1}$ (99)	
$v(0.09375)$	1.974	$1.27074429 \times 10^{-1}$ (12)	$1.2707443884 \times 10^{-1}$ (11)	
$v(0.125)$	1.982	$1.52547825 \times 10^{-1}$ (19)	$1.5254784047 \times 10^{-1}$ (13)	2.6×10^{-9}
$v(0.15625)$	1.986	$1.69611146 \times 10^{-1}$ (27)	$1.6961116685 \times 10^{-1}$ (14)	
$v(0.1875)$	1.989	$1.78781427 \times 10^{-1}$ (33)	$1.7878145314 \times 10^{-1}$ (14)	2.9×10^{-9}
$v(0.2265625)$	1.991	$1.80246732 \times 10^{-1}$ (39)	$1.8024676315 \times 10^{-1}$ (13)	
$v(0.234375)$	1.991	$1.79335221 \times 10^{-1}$ (39)	$1.7933525204 \times 10^{-1}$ (13)	
$v(0.25)$	1.991	$1.76415067 \times 10^{-1}$ (40)	$1.7641509929 \times 10^{-1}$ (13)	8×10^{-10}
$v(0.3125)$	1.992	$1.52055790 \times 10^{-1}$ (38)	$1.5205581979 \times 10^{-1}$ (11)	3×10^{-10}
$v(0.375)$	1.992	$1.12147740 \times 10^{-1}$ (28)	$1.12147762304 \times 10^{-1}$ (88)	1.1×10^{-9}
$v(0.4375)$	1.986	6.2104805×10^{-2} (14)	$6.2104816129 \times 10^{-2}$ (70)	1.4×10^{-9}
$v(0.5)$	2.037	6.3603660×10^{-3} (35)	$6.360363306 \times 10^{-3}$ (47)	1.3×10^{-9}
$v(0.5625)$	2.003	$-5.1041711 \times 10^{-2}$ (21)	$-5.1041727578 \times 10^{-2}$ (21)	9.3×10^{-10}
$v(0.625)$	1.998	$-1.05615697 \times 10^{-1}$ (35)	$-1.05615725250 \times 10^{-1}$ (21)	7×10^{-10}
$v(0.6875)$	1.995	$-1.51622065 \times 10^{-1}$ (44)	$-1.51622100515 \times 10^{-1}$ (80)	5×10^{-10}
$v(0.75)$	1.990	$-1.81633527 \times 10^{-1}$ (42)	$-1.8163356055 \times 10^{-1}$ (15)	5×10^{-10}
$v(0.8046875)$	1.982	$-1.87987895 \times 10^{-1}$ (31)	$-1.8798791960 \times 10^{-1}$ (20)	
$v(0.8125)$	1.980	$-1.87021627 \times 10^{-1}$ (29)	$-1.8702164996 \times 10^{-1}$ (21)	1.1×10^{-9}
$v(0.859375)$	1.957	$-1.70041601 \times 10^{-1}$ (14)	$-1.7004161208 \times 10^{-1}$ (22)	
$v(0.875)$	1.935	$-1.598981777 \times 10^{-1}$ (96)	$-1.5989818510 \times 10^{-1}$ (22)	9×10^{-10}
$v(0.90625)$	1.403	$-1.326835167 \times 10^{-1}$ (19)	$-1.3268351784 \times 10^{-1}$ (34)	
$v(0.9375)$	2.098	$-9.64099445 \times 10^{-2}$ (37)	$-9.640994171 \times 10^{-2}$ (13)	2.9×10^{-10}
$v(0.9453125)$	2.077	$-8.59947983 \times 10^{-2}$ (42)	$-8.599479507 \times 10^{-2}$ (11)	
$v(0.953125)$	2.063	$-7.50701860 \times 10^{-2}$ (44)	$-7.507018258 \times 10^{-2}$ (10)	
$v(0.9609375)$	2.053	$-6.36545291 \times 10^{-2}$ (44)	$-6.3654525680 \times 10^{-2}$ (84)	
$v(0.96875)$	2.046	$-5.17683670 \times 10^{-2}$ (41)	$-5.1768363779 \times 10^{-2}$ (67)	

Table 10 Comparisons of ψ_{min}, Re = 10

Reference	Grid	p_o	RE	$-\psi_{min}$	U	D	R
[2]	41	2		0.1000	C: 4.5×10^{-4}	1.1×10^{-4}	4.0
[22]	64	6		0.100137061		2.4×10^{-5}	
[16]	1024	2	9	0.1001132	A: 1.5×10^{-6}	4.5×10^{-7}	3.3
This work	2048	2		0.10011261		1.4×10^{-7}	
This work	4096	2		0.10011271	B: 1.1×10^{-7}	3.8×10^{-8}	2.9
This work	8192	2		0.100112739	C: 1.1×10^{-8}	8.6×10^{-9}	1.3
This work	8192	2	1	0.100112747639	M: 5.4×10^{-11}	**0 = ref**	

Note: The bold value indicates the best result of this work for ψ_{min}.

Table 11 Results of the variables with extremes, Re = 100, 8192 × 8192 grid

T	p_U	T_p(GCI)	$T_c(U_c)$	$\lvert T_c$-[13]$\rvert$	$\lvert T_c$-[16]$\rvert$	$\lvert T_c$-[2]$\rvert$
u_{min}	1.998	$-2.1404228 \times 10^{-1}$ (12)	$-2.14042378471 \times 10^{-1}$ (93)	2.2×10^{-8}	6.8×10^{-7}	3.1×10^{-3}
$y(u_{min})$	1.958	$4.58087531 \times 10^{-1}$ (11)	$4.5808752216 \times 10^{-1}$ (17)	1.2×10^{-5}	4.1×10^{-4}	5.0×10^{-3}
v_{min}	1.979	$-2.53802956 \times 10^{-1}$ (63)	$-2.5380300509 \times 10^{-1}$ (48)	5.0×10^{-9}	1.0×10^{-6}	8.5×10^{-3}
$x(v_{min})$	2.007	$8.10429605 \times 10^{-1}$ (96)	$8.1042952821 \times 10^{-1}$ (26)	3.9×10^{-5}	3.7×10^{-4}	5.7×10^{-3}
v_{max}	2.001	$1.79572766 \times 10^{-1}$ (87)	$1.79572835865 \times 10^{-1}$ (36)	3.6×10^{-8}	2.2×10^{-8}	4.3×10^{-3}
$x(v_{max})$	2.090	$2.36980862 \times 10^{-1}$ (13)	$2.3698085154 \times 10^{-1}$ (42)	1.9×10^{-5}	1.6×10^{-4}	2.6×10^{-3}
ψ_{min}	1.994	$-1.03520930 \times 10^{-1}$ (31)	$-1.03520954815 \times 10^{-1}$ (70)	1.0×10^{-6}	2.4×10^{-7}	9.8×10^{-5}
$x(\psi_{min})$	2.062	$6.15747801 \times 10^{-1}$ (28)	$6.1574777876 \times 10^{-1}$ (62)	4.8×10^{-5}	4.6×10^{-4}	1.4×10^{-3}
$y(\psi_{min})$	1.991	$7.37307719 \times 10^{-1}$ (31)	$7.3730769417 \times 10^{-1}$ (10)	4.9×10^{-4}	7.7×10^{-6}	2.9×10^{-3}

Table 12 Profile of u at $x = 1/2$, Re = 100, and 8192 × 8192 grid

$u(y)$	p_U	T_h(GCI)	$T_c(U_c)$	$\lvert T_c$-[16]$\rvert$	$\lvert T_c$-[21]$\rvert$	$\lvert T_c$-[6]$\rvert$
$u(0.0546875)$	1.968	$-3.72199412 \times 10^{-2}$ (10)	$-3.7219940439 \times 10^{-2}$ (12)		4.2×10^{-4}	5.0×10^{-5}
$u(0.0625)$	1.960	$-4.197500033 \times 10^{-2}$ (93)	$-4.1974999599 \times 10^{-2}$ (13)	8.6×10^{-9}	7.5×10^{-5}	5.5×10^{-5}
$u(0.0703125)$	1.947	$-4.662721784 \times 10^{-2}$ (76)	$-4.6627217247 \times 10^{-2}$ (15)		2.7×10^{-4}	1.1×10^{-3}
$u(0.1015625)$	2.038	$-6.44106550 \times 10^{-2}$ (11)	$-6.4410655876 \times 10^{-2}$ (14)		3.9×10^{-4}	7.1×10^{-5}
$u(0.125)$	2.009	$-7.71254106 \times 10^{-2}$ (38)	$-7.7125413623 \times 10^{-2}$ (12)	1.5×10^{-8}		
$u(0.171875)$	2.000	$-1.01729014 \times 10^{-1}$ (13)	$-1.017290247186 \times 10^{-1}$ (22)		1.7×10^{-4}	2.3×10^{-4}
$u(0.1875)$	1.999	$-1.09816218 \times 10^{-1}$ (18)	$-1.098162326574 \times 10^{-1}$ (93)	1.9×10^{-8}		
$u(0.25)$	1.997	$-1.41930049 \times 10^{-1}$ (43)	$-1.41930083805 \times 10^{-1}$ (47)	2.0×10^{-8}		
$u(0.28125)$	1.997	$-1.57648570 \times 10^{-1}$ (59)	$-1.57648617151 \times 10^{-1}$ (68)		3.5×10^{-4}	1.0×10^{-3}

Table 12 (continued)

$u(y)$	p_U	T_h(GCI)	$T_c(U_c)$	$\lvert T_c$-[16]$\rvert$	$\lvert T_c$-[21]$\rvert$	$\lvert T_c$-[6]$\rvert$
$u(0.3125)$	1.997	$-1.72712349 \times 10^{-1}(76)$	$-1.72712410360 \times 10^{-1}$ (89)	1.9×10^{-8}		
$u(0.375)$	1.997	$-1.9847079 \times 10^{-1}$ (11)	$-1.9847087425 \times 10^{-1}$ (12)	1.5×10^{-8}		
$u(0.4375)$	1.998	$-2.1296230 \times 10^{-1}$ (13)	$-2.1296239959 \times 10^{-1}$ (11)	7.5×10^{-9}		
$u(0.453125)$	1.998	$-2.1397790 \times 10^{-1}$ (13)	$-2.13977999359 \times 10^{-1}$ (98)		2.2×10^{-5}	3.1×10^{-3}
$u(0.5)$	1.999	$-2.0914904 \times 10^{-1}$ (12)	$-2.09149139883 \times 10^{-1}$ (44)	2.0×10^{-9}	4.9×10^{-5}	3.3×10^{-3}
$u(0.5625)$	2.002	$-1.82080509 \times 10^{-1}$ (93)	$-1.82080583499 \times 10^{-1}$ (69)	1.2×10^{-8}		
$u(0.6171875)$	2.009	$-1.38809412 \times 10^{-1}$ (51)	$-1.3880945236 \times 10^{-1}$ (18)		9.1×10^{-4}	2.4×10^{-3}
$u(0.625)$	2.011	$-1.31256247 \times 10^{-1}$ (45)	$-1.3125628280 \times 10^{-1}$ (19)	1.8×10^{-8}		
$u(0.6875)$	1.858	$-6.02455778 \times 10^{-2}$ (60)	$-6.024557326 \times 10^{-2}$ (30)	2.1×10^{-8}		
$u(0.734375)$	1.982	4.149963×10^{-3} (38)	$4.14999313 \times 10^{-3}$ (25)		2.9×10^{-3}	8.3×10^{-4}
$u(0.75)$	1.986	2.7874431×10^{-2} (46)	$2.787446774 \times 10^{-2}$ (23)	2.0×10^{-8}		
$u(0.8125)$	1.998	$1.40425287 \times 10^{-1}$ (67)	$1.40425341250 \times 10^{-1}$ (59)	1.6×10^{-8}		
$u(0.8515625)$	2.004	$2.36444462 \times 10^{-1}$ (69)	$2.36444517847 \times 10^{-1}$ (95)		3.4×10^{-3}	4.9×10^{-3}
$u(0.875)$	2.007	$3.10557048 \times 10^{-1}$ (69)	$3.1055710375 \times 10^{-1}$ (18)	1.4×10^{-8}		
$u(0.9375)$	2.009	$5.97466641 \times 10^{-1}$ (74)	$5.9746670009 \times 10^{-1}$ (23)	6.0×10^{-9}		
$u(0.953125)$	2.007	$6.91182786 \times 10^{-1}$ (70)	$6.9118284193 \times 10^{-1}$ (18)		7.0×10^{-3}	4.0×10^{-3}
$u(0.9609375)$	2.006	$7.40710146 \times 10^{-1}$ (65)	$7.4071019760 \times 10^{-1}$ (15)		1.1×10^{-2}	3.5×10^{-3}
$u(0.96875)$	2.005	$7.91608801 \times 10^{-1}$ (58)	$7.9160884743 \times 10^{-1}$ (11)		1.4×10^{-2}	2.9×10^{-3}
$u(0.9765625)$	2.004	$8.43481616 \times 10^{-1}$ (48)	$8.43481654719 \times 10^{-1}$ (70)		6.5×10^{-3}	2.2×10^{-3}

Table 13 Profile of v at $y = 1/2$, Re = 100, and 8192 × 8192 grid

$v(x)$	p_U	T_h(GCI)	$T_c(U_c)$	$\lvert T_c$-[16]$\rvert$	$\lvert T_c$-[21]$\rvert$	$\lvert T_c$-[6]$\rvert$
$v(0.0625)$	2.007	9.4807577×10^{-2} (59)	$9.480762394 \times 10^{-2}$ (15)	7.9×10^{-9}	1.1×10^{-4}	2.5×10^{-3}
$v(0.0703125)$	2.007	$1.03598822 \times 10^{-1}$ (64)	$1.0359887271 \times 10^{-1}$ (16)		4.0×10^{-4}	2.7×10^{-3}
$v(0.078125)$	2.007	$1.11777070 \times 10^{-1}$ (69)	$1.1177712497 \times 10^{-1}$ (17)		9.2×10^{-4}	2.9×10^{-3}
$v(0.09375)$	2.006	$1.26384684 \times 10^{-1}$ (77)	$1.2638474477 \times 10^{-1}$ (18)		2.2×10^{-4}	3.2×10^{-3}
$v(0.125)$	2.005	$1.49242944 \times 10^{-1}$ (88)	$1.4924301495 \times 10^{-1}$ (18)	1.5×10^{-8}		
$v(0.15625)$	2.004	$1.64804329 \times 10^{-1}$ (95)	$1.6480440446 \times 10^{-1}$ (16)		4.0×10^{-4}	4.0×10^{-3}
$v(0.1875)$	2.003	$1.74342870 \times 10^{-1}$ (98)	$1.7434294806 \times 10^{-1}$ (12)	1.5×10^{-8}		
$v(0.2265625)$	2.002	$1.79355041 \times 10^{-1}$ (97)	$1.79355118957 \times 10^{-1}$ (55)		4.5×10^{-5}	4.3×10^{-3}
$v(0.234375)$	2.001	$1.79559287 \times 10^{-1}$ (96)	$1.79559364295 \times 10^{-1}$ (41)		4.1×10^{-5}	4.3×10^{-3}
$v(0.25)$	2.000	$1.79243268 \times 10^{-1}$ (95)	$1.79243344033 \times 10^{-1}$ (13)	1.6×10^{-8}		
$v(0.3125)$	1.997	$1.69132013 \times 10^{-1}$ (84)	$1.6913207989 \times 10^{-1}$ (11)	1.6×10^{-8}		
$v(0.375)$	1.990	$1.45730166 \times 10^{-1}$ (65)	$1.4573021717 \times 10^{-1}$ (23)	1.6×10^{-8}		
$v(0.4375)$	1.975	$1.08775850 \times 10^{-1}$ (37)	$1.0877587948 \times 10^{-1}$ (34)	1.5×10^{-8}		
$v(0.5)$	2.413	$5.75365733 \times 10^{-2}$ (23)	$5.753657180 \times 10^{-2}$ (28)	1.3×10^{-8}	3.7×10^{-5}	3.0×10^{-3}
$v(0.5625)$	2.023	-7.748456×10^{-3} (50)	$-7.74849575 \times 10^{-3}$ (42)	8.2×10^{-9}		
$v(0.625)$	2.009	-8.406663×10^{-2} (10)	$-8.406671073 \times 10^{-2}$ (36)	4.3×10^{-9}		
$v(0.6875)$	2.003	$-1.6301003 \times 10^{-1}$ (15)	$-1.6301014678 \times 10^{-1}$ (17)	3.7×10^{-9}		
$v(0.75)$	1.997	$-2.2782720 \times 10^{-1}$ (16)	$-2.2782732946 \times 10^{-1}$ (15)	1.6×10^{-8}		
$v(0.8046875)$	1.989	$-2.5354143 \times 10^{-1}$ (11)	$-2.5354151415 \times 10^{-1}$ (45)		5.8×10^{-5}	8.2×10^{-3}
$v(0.8125)$	1.986	$-2.53768533 \times 10^{-1}$ (97)	$-2.5376861016 \times 10^{-1}$ (49)	3.3×10^{-8}		
$v(0.859375)$	1.940	$-2.33712483 \times 10^{-1}$ (29)	$-2.3371250593 \times 10^{-1}$ (62)		1.4×10^{-3}	9.3×10^{-3}
$v(0.875)$	1.769	$-2.186908464 \times 10^{-1}$ (92)	$-2.1869085304 \times 10^{-1}$ (72)	4.1×10^{-8}		
$v(0.90625)$	2.064	$-1.77157812 \times 10^{-1}$ (20)	$-1.7715779592 \times 10^{-1}$ (46)		2.2×10^{-3}	8.0×10^{-3}
$v(0.9375)$	2.031	$-1.23318220 \times 10^{-1}$ (28)	$-1.2331819721 \times 10^{-1}$ (32)	2.7×10^{-8}		
$v(0.9453125)$	2.027	$-1.08509162 \times 10^{-1}$ (28)	$-1.0850914066 \times 10^{-1}$ (27)		4.4×10^{-3}	5.4×10^{-3}
$v(0.953125)$	2.024	$-9.3339087 \times 10^{-2}$ (26)	$-9.333906670 \times 10^{-2}$ (22)		2.2×10^{-3}	4.7×10^{-3}
$v(0.9609375)$	2.021	$-7.7902060 \times 10^{-2}$ (23)	$-7.790204196 \times 10^{-2}$ (18)		3.2×10^{-3}	4.0×10^{-3}
$v(0.96875)$	2.018	$-6.2292972 \times 10^{-2}$ (20)	$-6.229295665 \times 10^{-2}$ (13)		4.3×10^{-3}	3.2×10^{-3}

Table 14 Comparisons of $\psi_{\min}$, Re = 100

Reference	Grid	p_o	RE	$-\psi_{\min}$	U	D	R
[19]	Free	2		0.0977		5.8×10^{-3}	
[2]	41	2		0.1015	C: 4.1×10^{-3}	2.0×10^{-3}	2.0
[4]	51	1		0.1026		9.2×10^{-4}	
[10]	256	1		0.1030		5.2×10^{-4}	
[12]	5	6		0.10330		2.2×10^{-4}	
[22]	64	6		0.103384675		1.4×10^{-4}	
[3]	128	2		0.1034	C: 8.3×10^{-5}	1.2×10^{-4}	0.7
[8]	321	1		0.1034		1.2×10^{-4}	
[6]	129	2		0.103423		9.8×10^{-5}	
[9]	129	10		0.103512	B: 1.8×10^{-8}	9.0×10^{-6}	0.002
[21]	601	2	2	0.1035270		6.0×10^{-6}	
[21]	601	2		0.1035160	B: 8.5×10^{-6}	5.0×10^{-6}	1.7

Table 14 (continued)

Reference	Grid	p_o	RE	$-\psi_{\min}$	U	D	R
[11]	1024	2		0.103519		2.0×10^{-6}	
This work	2048	2		0.10352056		4.0×10^{-7}	
[16]	1024	2	9	0.1035212	A: 1.1×10^{-6}	2.4×10^{-7}	4.5
This work	4096	2		0.10352086	B: 2.9×10^{-7}	9.5×10^{-8}	3.1
This work	8192	2		0.103520930	C: 3.1×10^{-8}	2.5×10^{-8}	1.3
This work	8192	2	1	0.103520954815	M: 7.0×10^{-11}	**0 = ref**	

Note: The bold value indicates the best result of this work for $\psi_{\min}$.

Table 15 Results of the variables with extremes, Re = 400, 8192 × 8192 grid

T	p_U	T_p(GCI)	$T_c(U_c)$	$\lvert T_c$-[16]$\rvert$	$\lvert T_c$-[22]$\rvert$	$\lvert T_c$-[6]$\rvert$
$u_{\min}$	1.993	$-3.2872966 \times 10^{-1}$ (69)	$-3.287302104 \times 10^{-1}$ (17)	7.1×10^{-7}	8.4×10^{-3}	1.5×10^{-3}
$y(u_{\min})$	1.982	2.8002505×10^{-1} (19)	$2.800248939 \times 10^{-1}$ (13)	2.4×10^{-4}	1.2×10^{-3}	1.2×10^{-3}
$v_{\min}$	1.989	$-4.5406484 \times 10^{-1}$ (78)	$-4.540654575 \times 10^{-1}$ (32)	7.5×10^{-6}	1.4×10^{-2}	4.1×10^{-3}
$x(v_{\min})$	2.024	$8.62213948 \times 10^{-1}$ (88)	$8.6221387868 \times 10^{-1}$ (76)	3.9×10^{-4}	2.8×10^{-3}	2.8×10^{-3}
$v_{\max}$	1.993	3.0383208×10^{-1} (64)	$3.038325909 \times 10^{-1}$ (17)	2.8×10^{-7}	8.5×10^{-3}	1.8×10^{-3}
$x(v_{\max})$	1.994	2.2530802×10^{-1} (16)	$2.2530788784 \times 10^{-1}$ (38)	2.1×10^{-4}	9.1×10^{-3}	1.2×10^{-3}
$\psi_{\min}$	1.993	$-1.1398879 \times 10^{-1}$ (17)	$-1.1398892555 \times 10^{-1}$ (44)	5.6×10^{-8}	2.0×10^{-3}	8.0×10^{-5}
$x(\psi_{\min})$	1.999	5.5409689×10^{-1} (14)	$5.54096778612 \times 10^{-1}$ (75)	3.9×10^{-4}	8.4×10^{-3}	6.0×10^{-4}
$y(\psi_{\min})$	1.975	$6.05423380 \times 10^{-1}$ (78)	$6.0542331835 \times 10^{-1}$ (72)	4.7×10^{-5}	4.0×10^{-3}	7.7×10^{-5}

Table 16 Profile of u at $x = 1/2$, Re = 400, and 8192 × 8192 grid

$u(y)$	p_U	T_h(GCI)	$T_c(U_c)$	$\lvert T_c$-[16]$\rvert$	$\lvert T_c$-[21]$\rvert$	$\lvert T_c$-[6]$\rvert$
u(0.0546875)	1.969	-8.180474×10^{-2} (10)	$-8.18048222 \times 10^{-2}$ (12)		9.0×10^{-4}	5.5×10^{-5}
u(0.0625)	1.971	-9.259924×10^{-2} (12)	$-9.25993359 \times 10^{-2}$ (13)	7.6×10^{-8}	2.1×10^{-3}	6.1×10^{-5}
u(0.0703125)	1.973	$-1.0331787 \times 10^{-1}$ (14)	$-1.033179843 \times 10^{-1}$ (14)		4.8×10^{-4}	6.2×10^{-5}
u(0.1015625)	1.980	$-1.4613915 \times 10^{-1}$ (25)	$-1.461393464 \times 10^{-1}$ (19)		1.1×10^{-3}	1.9×10^{-5}
u(0.125)	1.983	$-1.7874786 \times 10^{-1}$ (35)	$-1.787481398 \times 10^{-1}$ (22)	8.9×10^{-8}		
u(0.171875)	1.988	$-2.4374610 \times 10^{-1}$ (59)	$-2.437465655 \times 10^{-1}$ (26)		3.5×10^{-4}	7.6×10^{-4}
u(0.1875)	1.989	$-2.6391673 \times 10^{-1}$ (66)	$-2.639172526 \times 10^{-1}$ (27)	5.3×10^{-8}		
u(0.25)	1.992	$-3.2122844 \times 10^{-1}$ (79)	$-3.212290736 \times 10^{-1}$ (22)	6.4×10^{-9}		
u(0.28125)	1.994	$-3.2871715 \times 10^{-1}$ (73)	$-3.287177328 \times 10^{-1}$ (16)		1.2×10^{-4}	1.5×10^{-3}
u(0.3125)	1.996	$-3.2025057 \times 10^{-1}$ (59)	$-3.2025104779 \times 10^{-1}$ (96)	4.2×10^{-8}		
u(0.375)	2.002	$-2.6630607 \times 10^{-1}$ (29)	$-2.6630630236 \times 10^{-1}$ (16)	4.8×10^{-8}		
u(0.4375)	2.016	$-1.9073044 \times 10^{-1}$ (10)	$-1.9073052313 \times 10^{-1}$ (61)	3.7×10^{-8}		
u(0.453125)	2.022	$-1.71451878 \times 10^{-1}$ (80)	$-1.7145194161 \times 10^{-1}$ (64)		3.5×10^{-4}	2.6×10^{-4}
u(0.5)	2.057	$-1.15053585 \times 10^{-1}$ (32)	$-1.1505361060 \times 10^{-1}$ (66)	1.7×10^{-8}	5.4×10^{-5}	2.8×10^{-4}
u(0.5625)	1.900	$-4.2568959 \times 10^{-2}$ (23)	$-4.256894175 \times 10^{-2}$ (82)	5.2×10^{-9}		
u(0.6171875)	1.973	2.1019144×10^{-2} (91)	$2.101921536 \times 10^{-2}$ (88)		1.1×10^{-3}	3.3×10^{-4}
u(0.625)	1.976	3.024293×10^{-2} (10)	$3.024301204 \times 10^{-2}$ (90)	8.0×10^{-9}		
u(0.6875)	1.986	1.0545582×10^{-1} (22)	$1.054559928 \times 10^{-1}$ (11)	1.7×10^{-8}		
u(0.734375)	1.990	1.6253696×10^{-1} (32)	$1.625372206 \times 10^{-1}$ (12)		2.3×10^{-3}	2.3×10^{-5}
u(0.75)	1.990	1.8130654×10^{-1} (36)	$1.813068313 \times 10^{-1}$ (13)	1.9×10^{-8}		
u(0.8125)	1.992	2.5220340×10^{-1} (52)	$2.522038212 \times 10^{-1}$ (15)	1.9×10^{-8}		
u(0.8515625)	1.993	2.9199508×10^{-1} (60)	$2.919955584 \times 10^{-1}$ (15)		1.1×10^{-3}	1.1×10^{-3}
u(0.875)	1.994	3.1682921×10^{-1} (62)	$3.168297012 \times 10^{-1}$ (14)	1.1×10^{-8}		
u(0.9375)	1.994	4.6957996×10^{-1} (43)	$4.6958030064 \times 10^{-1}$ (89)	1.0×10^{-7}		
u(0.953125)	1.995	5.6173911×10^{-1} (37)	$5.6173940107 \times 10^{-1}$ (71)		7.8×10^{-3}	2.8×10^{-3}
u(0.9609375)	1.995	6.2021499×10^{-1} (34)	$6.2021526388 \times 10^{-1}$ (62)		1.3×10^{-2}	2.7×10^{-3}
u(0.96875)	1.995	6.8675557×10^{-1} (31)	$6.8675582453 \times 10^{-1}$ (53)		1.9×10^{-2}	2.4×10^{-3}
u(0.9765625)	1.996	7.6030384×10^{-1} (27)	$7.6030405181 \times 10^{-1}$ (44)		9.5×10^{-3}	1.9×10^{-3}

Table 17 Profile of v at $y = 1/2$, Re = 400, and 8192 × 8192 grid

$v(x)$	p_U	T_h(GCI)	$T_c(U_c)$	$\lvert T_c$-[16]$\rvert$	$\lvert T_c$-[21]$\rvert$	$\lvert T_c$-[6]$\rvert$
v(0.0625)	1.994	1.8513195×10^{-1} (50)	$1.851323485 \times 10^{-1}$ (11)	5.8×10^{-8}	2.3×10^{-4}	1.5×10^{-3}
v(0.0703125)	1.994	1.9880845×10^{-1} (53)	$1.988088747 \times 10^{-1}$ (12)		5.9×10^{-4}	1.7×10^{-3}
v(0.078125)	1.994	2.1100116×10^{-1} (55)	$2.110015996 \times 10^{-1}$ (13)		1.3×10^{-3}	1.8×10^{-3}
v(0.09375)	1.993	2.3166137×10^{-1} (59)	$2.316618420 \times 10^{-1}$ (14)		2.4×10^{-4}	2.0×10^{-3}
v(0.125)	1.993	2.6225080×10^{-1} (64)	$2.622513126 \times 10^{-1}$ (16)	5.3×10^{-8}		
v(0.15625)	1.993	2.8351460×10^{-1} (67)	$2.835151411 \times 10^{-1}$ (17)		4.8×10^{-4}	2.3×10^{-3}

Table 17 (continued)

$v(x)$	p_U	T_h(GCI)	$T_c(U_c)$	$\lvert T_c$-[16]$\rvert$	$\lvert T_c$-[21]$\rvert$	$\lvert T_c$-[6]$\rvert$
$v(0.1875)$	1.993	2.9747871×10^{-1} (69)	$2.974792569 \times 10^{-1}$ (18)	2.7×10^{-8}		
$v(0.2265625)$	1.993	3.0382475×10^{-1} (66)	$3.038252849 \times 10^{-1}$ (17)		1.2×10^{-4}	1.8×10^{-3}
$v(0.234375)$	1.993	3.0344817×10^{-1} (65)	$3.034486917 \times 10^{-1}$ (17)		1.5×10^{-4}	1.7×10^{-3}
$v(0.25)$	1.993	3.0095954×10^{-1} (62)	$3.009600371 \times 10^{-1}$ (16)	7.1×10^{-9}		
$v(0.3125)$	1.993	2.6831061×10^{-1} (41)	$2.683109420 \times 10^{-1}$ (11)	1.8×10^{-8}		
$v(0.375)$	1.991	2.0657123×10^{-1} (18)	$2.0657137113 \times 10^{-1}$ (61)	1.9×10^{-8}		
$v(0.4375)$	1.730	$1.305716761 \times 10^{-1}$ (37)	$1.3057167871 \times 10^{-1}$ (33)	1.5×10^{-8}		
$v(0.5)$	2.002	5.2058152×10^{-2} (99)	$5.2058073549 \times 10^{-2}$ (77)	8.5×10^{-9}	4.2×10^{-5}	2.0×10^{-4}
$v(0.5625)$	2.000	-2.471438×10^{-2} (17)	$-2.4714516519 \times 10^{-2}$ (25)	2.5×10^{-9}		
$v(0.625)$	1.999	$-1.0088399 \times 10^{-1}$ (22)	$-1.00884163957 \times 10^{-1}$ (74)	1.0×10^{-10}		
$v(0.6875)$	2.000	$-1.8210903 \times 10^{-1}$ (25)	$-1.821092379008 \times 10^{-1}$ (55)	1.0×10^{-10}		
$v(0.75)$	2.001	$-2.8098993 \times 10^{-1}$ (35)	$-2.80990215343 \times 10^{-1}$ (66)	3.7×10^{-9}		
$v(0.8046875)$	1.997	$-3.8563188 \times 10^{-1}$ (68)	$-3.8563242927 \times 10^{-1}$ (71)		2.7×10^{-3}	3.5×10^{-4}
$v(0.8125)$	1.997	$-4.0004172 \times 10^{-1}$ (75)	$-4.0004231835 \times 10^{-1}$ (96)	3.2×10^{-8}		
$v(0.859375)$	1.991	$-4.5383122 \times 10^{-1}$ (93)	$-4.538319605 \times 10^{-1}$ (30)		6.8×10^{-5}	3.9×10^{-3}
$v(0.875)$	1.988	$-4.4901119 \times 10^{-1}$ (85)	$-4.490118720 \times 10^{-1}$ (37)	2.2×10^{-8}		
$v(0.90625)$	1.980	$-3.8983372 \times 10^{-1}$ (58)	$-3.898341752 \times 10^{-1}$ (43)		4.3×10^{-3}	
$v(0.9375)$	1.972	$-2.7035478 \times 10^{-1}$ (34)	$-2.703550433 \times 10^{-1}$ (35)	1.0×10^{-7}		
$v(0.9453125)$	1.972	$-2.3466422 \times 10^{-1}$ (30)	$-2.346644519 \times 10^{-1}$ (31)		1.1×10^{-2}	6.2×10^{-3}
$v(0.953125)$	1.973	$-1.9809185 \times 10^{-1}$ (26)	$-1.980920592 \times 10^{-1}$ (26)		5.3×10^{-3}	5.6×10^{-3}
$v(0.9609375)$	1.974	$-1.6141253 \times 10^{-1}$ (22)	$-1.614127065 \times 10^{-1}$ (21)		7.6×10^{-3}	4.8×10^{-3}
$v(0.96875)$	1.975	$-1.2537388 \times 10^{-1}$ (18)	$-1.253740214 \times 10^{-1}$ (16)		9.7×10^{-3}	3.9×10^{-3}

Table 18 Comparisons of $\psi_{\min}$, Re = 400

Reference	Grid	p_o	RE	$-\psi_{\min}$	U	D	R
[4]	51	1		0.1014		1.3×10^{-2}	
[2]	41	2		0.1017	B: 3.4×10^{-2}	1.2×10^{-2}	2.8
[19]	Free	2		0.1088		5.2×10^{-3}	
[22]	64	6		0.112033208		2.0×10^{-3}	
[10]	256	1		0.1121		1.9×10^{-3}	
[7]	141	2		0.11297	B: 3.2×10^{-3}	1.0×10^{-3}	3.1
[8]	321	1		0.1136		3.9×10^{-4}	
[12]	5	6		0.11389		9.9×10^{-5}	
[6]	257	2		0.113909		8.0×10^{-5}	
[21]	601	2		0.1139640	C: 3.2×10^{-5}	2.5×10^{-5}	1.3
[7]	141	2	1	0.11401		2.1×10^{-5}	
This work	2048	2		0.1139868		2.1×10^{-6}	
This work	4096	2		0.1139884	B: 1.6×10^{-6}	5.3×10^{-7}	3.0
[21]	601	2	2	0.1139894		4.7×10^{-7}	
This work	8192	2		0.11398879	C: 1.7×10^{-7}	1.4×10^{-7}	1.3
[16]	1024	2	9	0.11398887	A: 3.1×10^{-7}	5.6×10^{-8}	5.6
This work	8192	2	1	0.11398892555	M: 4.4×10^{-10}	**0 = ref**	

Note: The bold value indicates the best result of this work for $\psi_{\min}$.

Table 19 Results of the variables with extremes, Re = 1000, 8192 × 8192 grid

T	p_U	T_p(GCI)	$T_c(U_c)$	$\lvert T_c$-[24]$\rvert$	$\lvert T_c$-[13]$\rvert$	$\lvert T_c$-[6]$\rvert$
$u_{\min}$	1.993	-3.885683×10^{-1} (19)	$-3.885697938 \times 10^{-1}$ (47)	6.2×10^{-9}	6.2×10^{-9}	5.7×10^{-3}
$y(u_{\min})$	1.993	1.7169710×10^{-1} (39)	$1.716967913 \times 10^{-1}$ (10)	3.2×10^{-6}	3.2×10^{-6}	1.8×10^{-4}
$v_{\min}$	1.994	-5.270754×10^{-1} (24)	$-5.270772755 \times 10^{-1}$ (58)	2.4×10^{-8}	1.8×10^{-7}	1.2×10^{-2}
$x(v_{\min})$	2.149	$9.092470009 \times 10^{-1}$ (89)	$9.0924699426 \times 10^{-1}$ (45)	4.7×10^{-5}	4.7×10^{-5}	3.0×10^{-3}
$v_{\max}$	1.992	3.769432×10^{-1} (18)	$3.769447085 \times 10^{-1}$ (58)	8.5×10^{-9}	8.5×10^{-9}	6.0×10^{-3}
$x(v_{\max})$	1.985	1.5783679×10^{-1} (34)	$1.578365250 \times 10^{-1}$ (19)	3.7×10^{-5}	3.7×10^{-5}	1.6×10^{-3}
$\psi_{\min}$	1.991	$-1.1893624 \times 10^{-1}$ (47)	$-1.189366115 \times 10^{-1}$ (15)	9.4×10^{-4}	1.2×10^{-8}	1.0×10^{-3}
$x(\psi_{\min})$	1.980	5.3079022×10^{-1} (14)	$5.307901107 \times 10^{-1}$ (10)	2.1×10^{-4}	9.9×10^{-6}	5.1×10^{-4}
$y(\psi_{\min})$	2.003	5.6524067×10^{-1} (14)	$5.6524055787 \times 10^{-1}$ (15)	2.4×10^{-4}	4.1×10^{-5}	2.7×10^{-3}

Table 20 Profile of u at $x = 1/2$, Re = 1000, and 8192 × 8192 grid

$u(y)$	p_U	T_h(GCI)	$T_c(U_c)$	$\lvert T_c$-[16]$\rvert$	$\lvert T_c$-[15]$\rvert$	$\lvert T_c$-[6]$\rvert$
$u(0.0546875)$	1.989	$-1.8125321 \times 10^{-1}$ (95)	$-1.812539636 \times 10^{-1}$ (38)			1.6×10^{-4}
$u(0.0625)$	1.990	-2.023291×10^{-1} (11)	$-2.023299884 \times 10^{-1}$ (42)	6.0×10^{-8}	6.0×10^{-5}	3.7×10^{-4}
$u(0.0703125)$	1.990	-2.229271×10^{-1} (12)	$-2.229280980 \times 10^{-1}$ (45)			7.3×10^{-4}
$u(0.1015625)$	1.992	-3.003688×10^{-1} (19)	$-3.003703285 \times 10^{-1}$ (55)		8.0×10^{-5}	3.1×10^{-3}
$u(0.125)$	1.993	-3.478431×10^{-1} (22)	$-3.478448222 \times 10^{-1}$ (58)	2.8×10^{-7}		
$u(0.171875)$	1.994	-3.885676×10^{-1} (20)	$-3.885692325 \times 10^{-1}$ (47)			5.7×10^{-3}

Table 20 (continued)

$u(y)$	p_U	T_h(GCI)	$T_c(U_c)$	$\lvert T_c$-[16]$\rvert$	$\lvert T_c$-[15]$\rvert$	$\lvert T_c$-[6]$\rvert$
$u(0.1875)$	1.994	-3.844078×10^{-1} (17)	$-3.844092069 \times 10^{-1}$ (41)	1.9×10^{-7}		
$u(0.25)$	1.992	$-3.1894525 \times 10^{-1}$ (89)	$-3.189459630 \times 10^{-1}$ (26)	1.4×10^{-7}		
$u(0.28125)$	1.991	$-2.8042785 \times 10^{-1}$ (76)	$-2.804284473 \times 10^{-1}$ (24)		2.8×10^{-5}	2.4×10^{-3}
$u(0.3125)$	1.991	$-2.4569306 \times 10^{-1}$ (71)	$-2.456936257 \times 10^{-1}$ (23)	7.4×10^{-8}		
$u(0.375)$	1.991	$-1.8373161 \times 10^{-1}$ (58)	$-1.837320753 \times 10^{-1}$ (20)	2.5×10^{-8}		
$u(0.4375)$	1.989	$-1.2341016 \times 10^{-1}$ (35)	$-1.234104382 \times 10^{-1}$ (15)	2.2×10^{-8}		
$u(0.453125)$	1.988	$-1.0817529 \times 10^{-1}$ (30)	$-1.081755212 \times 10^{-1}$ (13)			1.7×10^{-3}
$u(0.5)$	1.979	-6.205605×10^{-2} (12)	$-6.205614393 \times 10^{-2}$ (94)	1.4×10^{-8}	6.1×10^{-6}	1.3×10^{-3}
$u(0.5625)$	2.009	5.6167×10^{-4} (11)	5.6176057×10^{-4} (37)	3.9×10^{-8}		
$u(0.6171875)$	1.999	5.700436×10^{-2} (32)	$5.700461645 \times 10^{-2}$ (18)			1.5×10^{-5}
$u(0.625)$	1.998	6.524839×10^{-2} (35)	$6.524867230 \times 10^{-2}$ (26)	7.0×10^{-8}		
$u(0.6875)$	1.995	1.3357199×10^{-1} (60)	$1.335724704 \times 10^{-1}$ (10)	1.0×10^{-7}		
$u(0.734375)$	1.994	1.8864358×10^{-1} (80)	$1.886442145 \times 10^{-1}$ (17)		3.4×10^{-5}	1.5×10^{-3}
$u(0.75)$	1.994	2.0791378×10^{-1} (87)	$2.079144768 \times 10^{-1}$ (19)	1.3×10^{-7}		
$u(0.8125)$	1.993	2.884412×10^{-1} (12)	$2.884422264 \times 10^{-1}$ (33)	1.7×10^{-7}		
$u(0.8515625)$	1.992	3.371763×10^{-1} (15)	$3.371775527 \times 10^{-1}$ (44)			4.1×10^{-3}
$u(0.875)$	1.992	3.625438×10^{-1} (17)	$3.625451805 \times 10^{-1}$ (52)	2.2×10^{-7}		
$u(0.9375)$	1.986	4.229307×10^{-1} (17)	$4.229320227 \times 10^{-1}$ (87)	7.7×10^{-8}		
$u(0.953125)$	1.979	4.724491×10^{-1} (14)	$4.72450225 \times 10^{-1}$ (11)		6.0×10^{-5}	6.4×10^{-3}
$u(0.9609375)$	1.974	5.171830×10^{-1} (12)	$5.17183995 \times 10^{-1}$ (11)			6.0×10^{-3}
$u(0.96875)$	1.970	5.803655×10^{-1} (11)	$5.80366380 \times 10^{-1}$ (12)		5.6×10^{-5}	5.5×10^{-3}
$u(0.9765625)$	1.968	6.6397203×10^{-1} (91)	$6.63972748 \times 10^{-1}$ (11)			4.7×10^{-3}

Table 21 Profile of v at $y = 1/2$, Re = 1000, and 8192 × 8192 grid

$v(x)$	p_U	T_h(GCI)	$T_c(U_c)$	$\lvert T_c$-[16]$\rvert$	$\lvert T_c$-[15]$\rvert$	$\lvert T_c$-[6]$\rvert$
$v(0.0625)$	1.989	2.807042×10^{-1} (17)	$2.807055755 \times 10^{-1}$ (70)	1.2×10^{-7}		5.9×10^{-3}
$v(0.0703125)$	1.989	2.962922×10^{-1} (18)	$2.962936019 \times 10^{-1}$ (71)		7.4×10^{-5}	6.2×10^{-3}
$v(0.078125)$	1.989	3.099493×10^{-1} (18)	$3.099507872 \times 10^{-1}$ (72)			6.4×10^{-3}
$v(0.09375)$	1.990	3.329768×10^{-1} (19)	$3.329783441 \times 10^{-1}$ (72)		7.8×10^{-5}	6.7×10^{-3}
$v(0.125)$	1.991	3.650400×10^{-1} (20)	$3.650415794 \times 10^{-1}$ (69)	2.2×10^{-7}		
$v(0.15625)$	1.992	3.769157×10^{-1} (19)	$3.769171770 \times 10^{-1}$ (58)			6.0×10^{-3}
$v(0.1875)$	1.993	3.678512×10^{-1} (16)	$3.678524990 \times 10^{-1}$ (44)	2.0×10^{-7}		
$v(0.2265625)$	1.993	3.340319×10^{-1} (12)	$3.340328680 \times 10^{-1}$ (29)		5.3×10^{-5}	3.3×10^{-3}
$v(0.234375)$	1.994	3.253866×10^{-1} (11)	$3.253875192 \times 10^{-1}$ (26)			3.0×10^{-3}
$v(0.25)$	1.994	3.0710340×10^{-1} (97)	$3.071041720 \times 10^{-1}$ (22)	1.1×10^{-7}		
$v(0.3125)$	1.995	2.3126780×10^{-1} (65)	$2.312683189 \times 10^{-1}$ (13)	7.1×10^{-8}		
$v(0.375)$	1.996	1.6056381×10^{-1} (45)	$1.6056416650 \times 10^{-1}$ (62)	5.4×10^{-8}		
$v(0.4375)$	2.001	9.296911×10^{-2} (22)	$9.2969289717 \times 10^{-2}$ (51)	2.0×10^{-8}		
$v(0.5)$	1.871	2.5799473×10^{-2} (17)	$2.579946013 \times 10^{-2}$ (76)	1.3×10^{-10}	5.4×10^{-7}	5.4×10^{-4}
$v(0.5625)$	1.986	-4.184046×10^{-2} (25)	$-4.18406568 \times 10^{-2}$ (13)	2.3×10^{-8}		
$v(0.625)$	1.990	$-1.1079783 \times 10^{-1}$ (48)	$-1.107982142 \times 10^{-1}$ (18)	8.6×10^{-8}		
$v(0.6875)$	1.991	$-1.8167907 \times 10^{-1}$ (74)	$-1.816796602 \times 10^{-1}$ (24)	4.0×10^{-8}		
$v(0.75)$	1.992	-2.533806×10^{-1} (10)	$-2.533813815 \times 10^{-1}$ (30)	1.2×10^{-7}		
$v(0.8046875)$	1.991	-3.201954×10^{-1} (10)	$-3.201962274 \times 10^{-1}$ (34)			5.4×10^{-4}
$v(0.8125)$	1.990	$-3.31565806 \times 10^{-1}$ (98)	$-3.315665821 \times 10^{-1}$ (35)	1.2×10^{-7}		
$v(0.859375)$	1.993	-4.263892×10^{-1} (12)	$-4.263901668 \times 10^{-1}$ (33)		5.0×10^{-5}	2.6×10^{-4}
$v(0.875)$	1.994	-4.677741×10^{-1} (17)	$-4.677754629 \times 10^{-1}$ (36)	1.4×10^{-7}		
$v(0.90625)$	1.994	-5.264155×10^{-1} (27)	$-5.264176615 \times 10^{-1}$ (55)			1.1×10^{-2}
$v(0.9375)$	1.992	-4.561505×10^{-1} (23)	$-4.561523048 \times 10^{-1}$ (71)	2.4×10^{-7}		
$v(0.9453125)$	1.991	-4.102923×10^{-1} (21)	$-4.102939831 \times 10^{-1}$ (68)		1.1×10^{-4}	1.8×10^{-2}
$v(0.953125)$	1.991	-3.551312×10^{-1} (18)	$-3.551326710 \times 10^{-1}$ (62)			1.8×10^{-2}
$v(0.9609375)$	1.991	-2.933786×10^{-1} (16)	$-2.933798397 \times 10^{-1}$ (54)		8.0×10^{-5}	1.7×10^{-2}
$v(0.96875)$	1.991	-2.283407×10^{-1} (13)	$-2.283417650 \times 10^{-1}$ (43)			1.5×10^{-2}

Table 22 Comparisons of $\psi_{\min}$, Re = 1000

Reference	Grid	p_o	RE	$-\psi_{\min}$	U	D	R
This work	16	2		0.0845		3.9×10^{-2}	
[4]	51	1		0.0977		2.1×10^{-2}	
This work	32	2		0.1019	B: 7.2×10^{-3}	1.7×10^{-2}	0.4
This work	64	2		0.113	C: 2.8×10^{-2}	5.9×10^{-3}	4.7
[3]	128	2		0.114	B: 6.8×10^{-3}	4.9×10^{-3}	1.4
[19]	Free	2		0.1143		4.6×10^{-3}	
[7]	141	2		0.11603	C: 3.7×10^{-3}	2.9×10^{-3}	1.3
[8]	321	1		0.1173		1.6×10^{-3}	

Table 22 (continued)

Reference	Grid	p_o	RE	$-\psi_{\min}$	U	D	R
[5]	101	2		0.1175	C: 2.2×10^{-3}	1.4×10^{-3}	1.5
This work	128	2		0.1175	C: 2.7×10^{-3}	1.4×10^{-3}	1.9
[18]	257	3		0.117610	B: 2.7×10^{-4}	1.3×10^{-3}	0.2
[10]	256	1		0.1178		1.1×10^{-3}	
[6]	129	2		0.117929		1.0×10^{-3}	
[23]	50	7		0.118		9.4×10^{-4}	
This work	256	2		0.11856	C: 5.1×10^{-4}	3.8×10^{-4}	1.4
[5]	101	2	1	0.1193		3.6×10^{-4}	
This work	128	2	1	0.11923	M: 4.2×10^{-4}	2.9×10^{-4}	1.4
[14]	601	2		0.118781	C: 2.0×10^{-4}	1.6×10^{-4}	1.3
[11]	1024	2		0.118821	B: 7.2×10^{-4}	1.2×10^{-4}	6.2
This work	512	2		0.11884	C: 1.2×10^{-4}	9.7×10^{-5}	1.2
[21]	601	2		0.1188660	C: 8.5×10^{-5}	7.1×10^{-5}	1.2
[9]	129	8		0.119004		6.7×10^{-5}	
[17]	1025	2		0.118888		4.9×10^{-5}	
This work	1024	2		0.118913	C: 2.9×10^{-5}	2.4×10^{-5}	1.2
[7]	141	2	2	0.11896		2.3×10^{-5}	
[15]	1024	2		0.11892	C: 3.0×10^{-5}	1.7×10^{-5}	1.8
[22]	64	6		0.118950978		1.4×10^{-5}	
This work	256	2	1	0.118949	M: 2.1×10^{-5}	1.2×10^{-5}	1.7
[12]	257	8		0.118930	A: 1×10^{-5}	6.6×10^{-6}	1.5
This work	2048	2		0.1189307	C: 7.3×10^{-6}	5.9×10^{-6}	1.2
[14]	601	2	2	0.118942		5.4×10^{-6}	
[21]	601	2	2	0.1189329		3.7×10^{-6}	
This work	4096	2		0.1189351	C: 1.9×10^{-6}	1.5×10^{-6}	1.3
This work	512	2	1	0.1189380	M: 1.5×10^{-6}	1.4×10^{-6}	1.1
This work	8192	2		0.11893624	C: 4.7×10^{-7}	3.7×10^{-7}	1.3
[16]	1024	2	9	0.118936708	A: 3.1×10^{-8}	9.7×10^{-8}	0.3
This work	1024	2	1	0.1189365352	M: 5.0×10^{-9}	7.6×10^{-8}	0.1
This work	2048	2	1	0.1189365726	M: 6.1×10^{-9}	3.9×10^{-8}	0.2
[13]	161	160		0.1189366	A: $<1 \times 10^{-7}$	1.2×10^{-8}	8.7
This work	4096	2	1	0.1189366070	M: 5.8×10^{-9}	4.5×10^{-9}	1.3
[20]	2048	2	9	0.1189366104	A: 5×10^{-10}	1.1×10^{-9}	0.5
This work	8192	2	9	0.1189366107	O: 6.5×10^{-9}	8×10^{-10}	8.1
This work	8192	2	1	0.1189366115	M: 1.5×10^{-9}	**0 = ref**	

Note: The bold value indicates the best result of this work for $\psi_{\min}$.

Table 23 Results of the variables with extremes, Re = 3200, 8192 × 8192 grid

T	p_U	T_p(GCI)	$T_c(U_c)$	$\lvert T_c$-[6]$\rvert$	$\lvert T_c$-[19]$\rvert$	$\lvert T_c$-[18]$\rvert$
$u_{\min}$	1.998	-4.358960×10^{-1} (72)	$-4.359017581 \times 10^{-1}$ (45)	1.7×10^{-2}	1.8×10^{-2}	5.4×10^{-3}
$y(u_{\min})$	2.013	9.312987×10^{-2} (84)	$9.31292031 \times 10^{-2}$ (41)	8.4×10^{-3}		6.7×10^{-4}
$v_{\min}$	2.001	-5.684548×10^{-1} (92)	$-5.684622048 \times 10^{-1}$ (36)	2.8×10^{-2}	2.5×10^{-2}	
$x(v_{\min})$	2.034	9.4768283×10^{-1} (26)	$9.476830297 \times 10^{-1}$ (31)	2.4×10^{-3}		
$v_{\max}$	1.994	4.329990×10^{-1} (67)	$4.33004351 \times 10^{-1}$ (15)	5.3×10^{-3}	1.7×10^{-2}	6.0×10^{-3}
$x(v_{\max})$	1.989	9.675923×10^{-2} (70)	$9.67586709 \times 10^{-2}$ (28)	3.0×10^{-3}		9.4×10^{-4}
$\psi_{\min}$	1.995	-1.218195×10^{-1} (17)	$-1.218208301 \times 10^{-1}$ (30)	1.4×10^{-3}	1.7×10^{-4}	6.7×10^{-4}
$x(\psi_{\min})$	1.851	5.1787832×10^{-1} (10)	$5.178782388 \times 10^{-1}$ (53)	1.4×10^{-3}	3.8×10^{-4}	2.3×10^{-3}
$y(\psi_{\min})$	2.047	5.4031954×10^{-1} (29)	$5.403193098 \times 10^{-1}$ (49)	6.6×10^{-3}	4.8×10^{-4}	1.2×10^{-3}

Table 24 Profile of u at $x = 1/2$, Re = 3200, and 8192 × 8192 grid

$u(y)$	p_U	T_h(GCI)	$T_c(U_c)$	$\lvert T_c$-[6]$\rvert$	$\lvert T_c$-[21]$\rvert$
$u(0.0546875)$	2.004	-3.564998×10^{-1} (74)	$-3.56505759 \times 10^{-1}$ (10)	3.2×10^{-2}	3.5×10^{-3}
$u(0.0625)$	2.003	-3.854170×10^{-1} (81)	$-3.854234382 \times 10^{-1}$ (79)	3.2×10^{-2}	1.5×10^{-3}
$u(0.0703125)$	2.002	-4.083095×10^{-1} (84)	$-4.083161862 \times 10^{-1}$ (50)	3.0×10^{-2}	2.2×10^{-4}
$u(0.1015625)$	1.997	-4.329149×10^{-1} (67)	$-4.329202000 \times 10^{-1}$ (71)	1.4×10^{-2}	1.5×10^{-3}
$u(0.125)$	1.994	-4.050760×10^{-1} (50)	$-4.05080011 \times 10^{-1}$ (11)		
$u(0.171875)$	1.993	-3.455593×10^{-1} (44)	$-3.45562839 \times 10^{-1}$ (11)	2.3×10^{-2}	1.1×10^{-3}
$u(0.1875)$	1.994	-3.303570×10^{-1} (44)	$-3.30360479 \times 10^{-1}$ (10)		
$u(0.25)$	1.993	-2.721302×10^{-1} (35)	$-2.721330167 \times 10^{-1}$ (95)		
$u(0.28125)$	1.992	-2.426159×10^{-1} (31)	$-2.426183383 \times 10^{-1}$ (92)	1.7×10^{-3}	1.2×10^{-3}
$u(0.3125)$	1.991	-2.131702×10^{-1} (27)	$-2.131723451 \times 10^{-1}$ (88)		
$u(0.375)$	1.988	-1.545286×10^{-1} (19)	$-1.545300485 \times 10^{-1}$ (81)		
$u(0.4375)$	1.982	-9.59116×10^{-2} (11)	$-9.59124947 \times 10^{-2}$ (72)		
$u(0.453125)$	1.978	-8.121576×10^{-2} (87)	$-8.12164536 \times 10^{-2}$ (70)	5.4×10^{-3}	4.2×10^{-4}
$u(0.5)$	1.932	-3.689763×10^{-2} (27)	$-3.68978380 \times 10^{-2}$ (66)	5.8×10^{-3}	2.2×10^{-6}

Table 24 (continued)

$u(y)$	p_U	T_h(GCI)	$T_c(U_c)$	$\lvert T_c$-[6]$\rvert$	$\lvert T_c$-[21]$\rvert$
$u(0.5625)$	2.024	2.314209×10^{-2} (56)	$2.31425353 \times 10^{-2}$ (49)		
$u(0.6171875)$	2.008	7.72072×10^{-2} (13)	$7.72082043 \times 10^{-2}$ (38)	5.7×10^{-3}	7.9×10^{-4}
$u(0.625)$	2.007	8.50925×10^{-2} (14)	$8.50936354 \times 10^{-2}$ (36)		
$u(0.6875)$	2.002	1.501251×10^{-1} (23)	$1.501269457 \times 10^{-1}$ (17)		
$u(0.734375)$	2.000	2.018140×10^{-1} (30)	$2.0181640118 \times 10^{-1}$ (24)	3.9×10^{-3}	1.7×10^{-3}
$u(0.75)$	1.999	2.197420×10^{-1} (32)	$2.197445856 \times 10^{-1}$ (10)		
$u(0.8125)$	1.997	2.957923×10^{-1} (42)	$2.957956862 \times 10^{-1}$ (48)		
$u(0.8515625)$	1.996	3.481881×10^{-1} (49)	$3.481919839 \times 10^{-1}$ (76)	1.4×10^{-3}	9.1×10^{-4}
$u(0.875)$	1.995	3.820091×10^{-1} (54)	$3.820133969 \times 10^{-1}$ (95)		
$u(0.9375)$	1.993	4.573942×10^{-1} (73)	$4.57399956 \times 10^{-1}$ (18)		
$u(0.953125)$	1.991	4.617986×10^{-1} (73)	$4.61804432 \times 10^{-1}$ (24)	7.9×10^{-4}	8.0×10^{-4}
$u(0.9609375)$	1.988	4.654144×10^{-1} (69)	$4.65419893 \times 10^{-1}$ (30)	5.0×10^{-5}	6.8×10^{-4}
$u(0.96875)$	1.981	4.809878×10^{-1} (60)	$4.80992545 \times 10^{-1}$ (42)	2.0×10^{-3}	7.6×10^{-3}
$u(0.9765625)$	1.967	5.277196×10^{-1} (47)	$5.27723283 \times 10^{-1}$ (57)	4.6×10^{-3}	8.3×10^{-3}

Table 25 Profile of v at $y = 1/2$, Re = 3200, and 8192 × 8192 grid

$v(x)$	p_U	T_h(GCI)	$T_c(U_c)$	$\lvert T_c$-[6]$\rvert$	$\lvert T_c$-[21]$\rvert$
$v(0.0625)$	1.992	3.961421×10^{-1} (72)	$3.96147846 \times 10^{-1}$ (20)	5.5×10^{-4}	1.3×10^{-3}
$v(0.0703125)$	1.993	4.112850×10^{-1} (74)	$4.11290906 \times 10^{-1}$ (19)	2.1×10^{-3}	3.9×10^{-4}
$v(0.078125)$	1.993	4.224527×10^{-1} (74)	$4.22458562 \times 10^{-1}$ (18)	3.4×10^{-3}	5.9×10^{-5}
$v(0.09375)$	1.994	4.327436×10^{-1} (70)	$4.32749196 \times 10^{-1}$ (15)	5.1×10^{-3}	9.5×10^{-4}
$v(0.125)$	1.995	4.155245×10^{-1} (56)	$4.15528945 \times 10^{-1}$ (11)		
$v(0.15625)$	1.995	3.772419×10^{-1} (47)	$3.772456521 \times 10^{-1}$ (90)	6.1×10^{-3}	2.0×10^{-3}
$v(0.1875)$	1.995	3.395198×10^{-1} (43)	$3.395232386 \times 10^{-1}$ (76)		
$v(0.2265625)$	1.996	2.965348×10^{-1} (38)	$2.965378729 \times 10^{-1}$ (55)	6.2×10^{-3}	1.1×10^{-3}
$v(0.234375)$	1.996	2.881511×10^{-1} (37)	$2.881540209 \times 10^{-1}$ (51)	6.3×10^{-3}	1.8×10^{-3}
$v(0.25)$	1.997	2.714568×10^{-1} (35)	$2.714596222 \times 10^{-1}$ (43)		
$v(0.3125)$	1.999	2.055142×10^{-1} (26)	$2.055162667 \times 10^{-1}$ (13)		
$v(0.375)$	2.002	1.409767×10^{-1} (18)	$1.409780956 \times 10^{-1}$ (11)		
$v(0.4375)$	2.008	7.741824×10^{-2} (98)	$7.74190257 \times 10^{-2}$ (30)		
$v(0.5)$	2.068	1.426181×10^{-2} (18)	$1.42619482 \times 10^{-2}$ (43)	4.3×10^{-3}	6.2×10^{-5}
$v(0.5625)$	1.975	-4.918058×10^{-2} (65)	$-4.91810882 \times 10^{-2}$ (59)		
$v(0.625)$	1.987	-1.137093×10^{-1} (15)	$-1.137104579 \times 10^{-1}$ (70)		
$v(0.6875)$	1.991	-1.802065×10^{-1} (23)	$-1.802083325 \times 10^{-1}$ (79)		
$v(0.75)$	1.993	-2.496053×10^{-1} (32)	$-2.496078969 \times 10^{-1}$ (88)		
$v(0.8046875)$	1.994	-3.136729×10^{-1} (41)	$-3.136761813 \times 10^{-1}$ (95)	1.8×10^{-3}	1.1×10^{-3}
$v(0.8125)$	1.994	-3.230943×10^{-1} (42)	$-3.230976756 \times 10^{-1}$ (95)		
$v(0.859375)$	1.995	-3.787502×10^{-1} (51)	$-3.787542882 \times 10^{-1}$ (96)	4.7×10^{-3}	1.2×10^{-3}
$v(0.875)$	1.995	-3.962701×10^{-1} (53)	$-3.96274295 \times 10^{-1}$ (10)		
$v(0.90625)$	1.990	-4.435044×10^{-1} (43)	$-4.43507863 \times 10^{-1}$ (16)	4.4×10^{-4}	2.7×10^{-3}
$v(0.9375)$	1.997	-5.496099×10^{-1} (78)	$-5.496162027 \times 10^{-1}$ (91)		
$v(0.9453125)$	2.000	-5.672294×10^{-1} (98)	$-5.6723728216 \times 10^{-1}$ (16)	2.7×10^{-2}	1.4×10^{-4}
$v(0.953125)$	2.003	-5.61005×10^{-1} (11)	$-5.61013978 \times 10^{-1}$ (11)	3.7×10^{-2}	5.0×10^{-3}
$v(0.9609375)$	2.005	-5.19777×10^{-1} (11)	$-5.19785368 \times 10^{-1}$ (21)	4.6×10^{-2}	1.5×10^{-2}
$v(0.96875)$	2.007	-4.397306×10^{-1} (99)	$-4.39738466 \times 10^{-1}$ (26)	5.0×10^{-2}	2.9×10^{-2}

Table 26 Comparisons of $\psi_{\min}$, Re = 3200

Reference	Grid	p_o	RE	$-\psi_{\min}$	U	D	R
[19]	Free	2		0.1160		5.8×10^{-3}	
[6]	129	2		0.120377		1.4×10^{-3}	
[18]	257	3		0.120475	B: 8.4×10^{-4}	1.4×10^{-3}	0.6
[5]	101	2		0.1210	C: 7.0×10^{-4}	8.2×10^{-4}	0.9
[9]	129	6		0.121154		6.7×10^{-4}	
[21]	601	2		0.1215660	C: 3.3×10^{-4}	2.6×10^{-4}	1.3
[5]	101	2	1	0.1217		1.2×10^{-4}	
This work	2048	2		0.121799		2.2×10^{-5}	
This work	4096	2		0.121815	B: 1.6×10^{-5}	5.8×10^{-6}	2.7
This work	8192	2		0.1218195	C: 1.7×10^{-6}	1.3×10^{-6}	1.3
[21]	601	2	2	0.1218198		1.0×10^{-6}	
This work	8192	2	1	0.1218208301	M: 3.0×10^{-9}	**0 = ref**	

Note: The bold value indicates the best result of this work for $\psi_{\min}$.

Table 27 Results of the variables with extremes, Re = 5000, 8192 × 8192 grid

T	p_U	T_p(GCI)	$T_c(U_c)$	$\lvert T_c$-[6]$\rvert$	$\lvert T_c$-[18]$\rvert$	$\lvert T_c$-[8]$\rvert$
u_{min}	2.000	-4.47304×10^{-1} (12)	$-4.473136506 \times 10^{-1}$ (21)	1.1×10^{-2}	5.8×10^{-3}	1.1×10^{-1}
$y(u_{min})$	2.013	7.42977×10^{-2} (11)	$7.42967560 \times 10^{-2}$ (56)	4.0×10^{-3}	9.7×10^{-5}	1.0×10^{-2}
v_{min}	2.002	-5.76124×10^{-1} (15)	$-5.76136016 \times 10^{-1}$ (10)	2.2×10^{-2}		
$x(v_{min})$	2.025	9.5746013×10^{-1} (47)	$9.574604998 \times 10^{-1}$ (43)	4.3×10^{-3}		
v_{max}	1.996	4.47500×10^{-1} (11)	$4.47508528 \times 10^{-1}$ (16)	1.1×10^{-2}	6.6×10^{-3}	
$x(v_{max})$	1.995	7.968888×10^{-2} (93)	$7.96881334 \times 10^{-2}$ (19)	1.6×10^{-3}	2.3×10^{-3}	
ψ_{min}	1.997	-1.222237×10^{-1} (28)	$-1.222258910 \times 10^{-1}$ (31)	6.5×10^{-6}	4.3×10^{-5}	2.6×10^{-4}
$x(\psi_{min})$	6.602	$5.1509378884 \times 10^{-1}$ (43)	$5.1509378902 \times 10^{-1}$ (17)	1.3×10^{-5}	4.1×10^{-4}	4.4×10^{-4}
$y(\psi_{min})$	2.039	5.3526230×10^{-1} (43)	$5.352619646 \times 10^{-1}$ (60)	6.1×10^{-4}	2.4×10^{-4}	1.0×10^{-4}

Table 27; in column $|T_c$-[6]$|$, the results of ψ_{min} and its coordinates are from Ref. [12], while those in column $|T_c$-[18]$|$ are from Ref. [21]. The results for Re = 5000 for the velocity profiles are displayed in Tables 28 and 29. Comparisons with other authors of ψ_{min} for Re = 5000 are presented in Table 30.

4.8 Re = 7500. The results for Re = 7500 for the variables with extremes based on the 8192 × 8192 grid are shown in Table 31. The results for Re = 7500 for the velocity profiles are displayed in Tables 32 and 33. Comparisons with other authors of ψ_{min} for Re = 7500 are presented in Table 34.

4.9 Re = 10,000. The streamlines of the solution for Re = 10,000 in the 2048 × 2048 grid are presented in Fig. 3. The results for Re = 10,000 for the variables with extremes based on the 8192 × 8192 grid are shown in Table 35. The results for Re = 10,000 for the velocity profiles are displayed in Tables 36 and 37. Comparisons with other authors of ψ_{min} for Re = 10,000 are presented in Table 38.

4.10 Discussion of the Results of Re = 1 to 10,000. The behavior of the equivalent apparent order (p_U) of the discretization error, calculated using Eq. (6), with grid refinement for four variables and Re = 1000 are shown in Fig. 4. The value of the equivalent apparent order in each grid is indicated by a symbol. In the grid with $h \approx 3.9 \times 10^{-3}$ (256 × 256 volumes) and smaller values of h, the equivalent apparent order is very close to 2, which is the theoretical order of accuracy (p_o) of the numerical approximations used here, as described in Sec. 3. In the finest grid ($h \approx 1.2 \times 10^{-4}$ with 8192 × 8192 volumes), the equivalent apparent order of the four variables is visually equal to 2. This behavior generally occurs for all other variables and for all Reynolds numbers. Therefore, it can be inferred that the GCI and U_c error estimates presented in Secs. 4.1–4.9 are reliable because the numerical solutions in the finest grids are already in the convergent range of the discretization error. Of the 585 p_U values, only 21 or 3.6% were outside the 1.90 to 2.10 range, corresponding to a variation of ±5% of p_o. In general, the higher the Reynolds number, the fewer values fell outside the range, that is, 9, 4, and 3, respectively, for Re = 1, 10, and 100; 1 or 2 values for Re = 400 to 5000; and zero for Re = 7500 and 10,000.

Comparing the results of this study with those in the literature (Table 1) revealed the following with respect to the order of magnitude of D: for the coordinates, it varied between 2 and 6; the minimum and maximum values of u and v varied between 1 and 9; for u and v profiles, it varied between 2 and 11; and for ψ_{min}, it varied between 2 and 10. These significant variations were to be

Table 28 Profile of u at $x = 1/2$, Re = 5000, and 8192 × 8192 grid

u(y)	p_U	T_h(GCI)	$T_c(U_c)$	$\lvert T_c$-[6]$\rvert$	$\lvert T_c$-[21]$\rvert$	$\lvert T_c$-[14]$\rvert$
u(0.0546875)	2.003	-4.16830×10^{-1} (14)	$-4.16840867 \times 10^{-1}$ (13)	5.2×10^{-3}	1.5×10^{-3}	
u(0.0625)	2.001	-4.36816×10^{-1} (14)	$-4.368267382 \times 10^{-1}$ (74)	7.8×10^{-3}	8.3×10^{-4}	
u(0.0703125)	2.000	-4.46197×10^{-1} (13)	$-4.462075575 \times 10^{-1}$ (13)	9.8×10^{-3}	6.1×10^{-4}	
u(0.1015625)	1.996	-4.170803×10^{-1} (86)	$-4.17087182 \times 10^{-1}$ (12)	1.3×10^{-2}	1.9×10^{-4}	
u(0.125)	1.996	-3.839560×10^{-1} (81)	$-3.83962495 \times 10^{-1}$ (12)			
u(0.171875)	1.996	-3.383484×10^{-1} (76)	$-3.38354434 \times 10^{-1}$ (11)	7.9×10^{-3}	8.5×10^{-4}	
u(0.1875)	1.996	-3.239140×10^{-1} (72)	$-3.23919765 \times 10^{-1}$ (11)			
u(0.25)	1.995	-2.653439×10^{-1} (57)	$-2.65348489 \times 10^{-1}$ (10)			
u(0.28125)	1.995	-2.361779×10^{-1} (50)	$-2.36181883 \times 10^{-1}$ (10)	7.6×10^{-3}	2.8×10^{-4}	
u(0.3125)	1.994	-2.070741×10^{-1} (43)	$-2.070775280 \times 10^{-1}$ (96)			
u(0.375)	1.992	-1.489428×10^{-1} (30)	$-1.489451975 \times 10^{-1}$ (89)			
u(0.4375)	1.987	-9.07345×10^{-2} (17)	$-9.07358520 \times 10^{-2}$ (81)			
u(0.453125)	1.984	-7.61325×10^{-2} (14)	$-7.61336001 \times 10^{-2}$ (79)	2.1×10^{-3}	9.3×10^{-4}	
u(0.5)	1.943	-3.208841×10^{-2} (36)	$-3.20886883 \times 10^{-2}$ (74)	1.7×10^{-3}	1.1×10^{-5}	1.9×10^{-4}
u(0.5625)	2.016	2.757053×10^{-2} (99)	$2.75713117 \times 10^{-2}$ (58)			
u(0.6171875)	2.006	8.12428×10^{-2} (22)	$8.12445326 \times 10^{-2}$ (47)	5.9×10^{-4}	5.6×10^{-4}	
u(0.625)	2.005	8.90646×10^{-2} (24)	$8.90665175 \times 10^{-2}$ (45)			
u(0.6875)	2.002	1.534948×10^{-1} (38)	$1.534978383 \times 10^{-1}$ (25)			
u(0.734375)	2.000	2.045923×10^{-1} (49)	$2.0459625315 \times 10^{-1}$ (40)	3.7×10^{-3}	1.0×10^{-4}	
u(0.75)	2.000	2.222964×10^{-1} (53)	$2.2230067105 \times 10^{-1}$ (42)			
u(0.8125)	1.998	2.973327×10^{-1} (70)	$2.973382843 \times 10^{-1}$ (46)			
u(0.8515625)	1.997	3.484147×10^{-1} (81)	$3.484211804 \times 10^{-1}$ (79)	1.3×10^{-2}	9.8×10^{-4}	
u(0.875)	1.997	3.812703×10^{-1} (88)	$3.81277366 \times 10^{-1}$ (10)			
u(0.9375)	1.996	4.69990×10^{-1} (12)	$4.69999440 \times 10^{-1}$ (18)			
u(0.953125)	1.995	4.78519×10^{-1} (12)	$4.78528880 \times 10^{-1}$ (23)	1.8×10^{-2}	5.3×10^{-4}	
u(0.9609375)	1.994	4.77917×10^{-1} (12)	$4.77926657 \times 10^{-1}$ (26)	1.8×10^{-2}	8.3×10^{-4}	
u(0.96875)	1.992	4.78249×10^{-1} (11)	$4.78257676 \times 10^{-1}$ (36)	1.7×10^{-2}	5.8×10^{-5}	
u(0.9765625)	1.984	4.968353×10^{-1} (94)	$4.96842773 \times 10^{-1}$ (56)	1.5×10^{-2}	4.7×10^{-3}	

Table 29 Profile of v at $y = 1/2$, Re = 5000, and 8192 × 8192 grid

$v(x)$	p_U	T_h(GCI)	$T_c(U_c)$	$\lvert T_c$-[6]$\rvert$	$\lvert T_c$-[21]$\rvert$	$\lvert T_c$-[14]$\rvert$
$v(0.0625)$	1.996	4.34346×10^{-1} (12)	$4.34355435 \times 10^{-1}$ (19)	9.9×10^{-3}	7.6×10^{-4}	
$v(0.0703125)$	1.996	4.43780×10^{-1} (12)	$4.43789460 \times 10^{-1}$ (18)	1.1×10^{-2}	4.9×10^{-4}	
$v(0.078125)$	1.996	4.47403×10^{-1} (11)	$4.47411790 \times 10^{-1}$ (16)	1.1×10^{-2}	6.1×10^{-4}	
$v(0.09375)$	1.996	4.40910×10^{-1} (10)	$4.40918307 \times 10^{-1}$ (14)	1.1×10^{-2}	2.2×10^{-4}	
$v(0.125)$	1.996	4.033439×10^{-1} (83)	$4.03350591 \times 10^{-1}$ (12)			
$v(0.15625)$	1.996	3.654076×10^{-1} (78)	$3.65413847 \times 10^{-1}$ (10)	1.2×10^{-2}	5.1×10^{-4}	
$v(0.1875)$	1.997	3.311736×10^{-1} (71)	$3.311793471 \times 10^{-1}$ (83)			
$v(0.2265625)$	1.998	2.894181×10^{-1} (62)	$2.894231248 \times 10^{-1}$ (58)	8.8×10^{-3}	1.1×10^{-3}	
$v(0.234375)$	1.998	2.811462×10^{-1} (61)	$2.811510448 \times 10^{-1}$ (53)	8.3×10^{-3}	2.5×10^{-4}	
$v(0.25)$	1.998	2.646922×10^{-1} (57)	$2.646967992 \times 10^{-1}$ (44)			
$v(0.3125)$	1.999	1.999526×10^{-1} (43)	$1.999560220 \times 10^{-1}$ (11)			
$v(0.375)$	2.001	1.365260×10^{-1} (30)	$1.365283554 \times 10^{-1}$ (16)			
$v(0.4375)$	2.006	7.39562×10^{-2} (17)	$7.39575603 \times 10^{-2}$ (37)			
$v(0.5)$	2.039	1.173233×10^{-2} (37)	$1.17326245 \times 10^{-2}$ (52)	2.3×10^{-3}	3.3×10^{-5}	3.3×10^{-5}
$v(0.5625)$	1.981	-5.077548×10^{-2} (97)	$-5.07762541 \times 10^{-2}$ (69)			
$v(0.625)$	1.991	-1.143112×10^{-1} (23)	$-1.143130313 \times 10^{-1}$ (80)			
$v(0.6875)$	1.994	-1.797070×10^{-1} (37)	$-1.797100257 \times 10^{-1}$ (89)			
$v(0.75)$	1.995	-2.478477×10^{-1} (52)	$-2.478518581 \times 10^{-1}$ (97)			
$v(0.8046875)$	1.996	-3.104230×10^{-1} (66)	$-3.10428291 \times 10^{-1}$ (10)	1.0×10^{-2}	7.7×10^{-4}	
$v(0.8125)$	1.996	-3.196402×10^{-1} (68)	$-3.19645667 \times 10^{-1}$ (10)			
$v(0.859375)$	1.997	-3.765183×10^{-1} (82)	$-3.76524812 \times 10^{-1}$ (10)	1.4×10^{-2}	1.1×10^{-3}	
$v(0.875)$	1.997	-3.953488×10^{-1} (88)	$-3.95355749 \times 10^{-1}$ (10)			
$v(0.90625)$	1.997	-4.302585×10^{-1} (93)	$-4.30265902 \times 10^{-1}$ (12)	1.6×10^{-2}	1.1×10^{-3}	
$v(0.9375)$	1.993	-5.055353×10^{-1} (77)	$-5.05541509 \times 10^{-1}$ (21)			
$v(0.9453125)$	1.996	-5.41029×10^{-1} (10)	$-5.41037295 \times 10^{-1}$ (16)	1.2×10^{-2}	5.0×10^{-3}	
$v(0.953125)$	2.000	-5.70337×10^{-1} (15)	$-5.703484303 \times 10^{-1}$ (15)	1.6×10^{-2}	2.2×10^{-3}	
$v(0.9609375)$	2.003	-5.71563×10^{-1} (18)	$-5.71578117 \times 10^{-1}$ (20)	2.1×10^{-2}	2.7×10^{-3}	
$v(0.96875)$	2.006	-5.21332×10^{-1} (19)	$-5.21346934 \times 10^{-1}$ (40)	2.4×10^{-2}	9.3×10^{-3}	

Table 30 Comparisons of $\psi_{\min}$, Re = 5000

Reference	Grid	p_o	RE	$-\psi_{\min}$	U	D	R
[4]	51	1		0.0861		3.6×10^{-2}	
[8]	161	1		0.0920		3.0×10^{-2}	
[6]	257	2		0.118966		3.3×10^{-3}	
[18]	257	3		0.121062	B: 1.2×10^{-3}	1.2×10^{-3}	1.0
[14]	601	2		0.121289	C: 1.2×10^{-3}	9.4×10^{-4}	1.3
[10]	256	1		0.1214		8.3×10^{-4}	
[17]	1025	2		0.121942		2.8×10^{-4}	
[15]	2048	2		0.12197	C: 1.7×10^{-5}	2.6×10^{-4}	0.1
[21]	1001	2		0.1220690	C: 6.3×10^{-4}	1.6×10^{-4}	4.0
[21]	1001	2	2	0.1222680		4.2×10^{-5}	
This work	2048	2		0.122190		3.6×10^{-5}	
This work	4096	2		0.122217	B: 2.7×10^{-5}	8.9×10^{-6}	3.0
[14]	601	2	2	0.122233		7.1×10^{-6}	
[12]	257	8		0.1222194	A: 1×10^{-5}	6.5×10^{-6}	1.5
This work	8192	2		0.1222237	C: 2.8×10^{-6}	2.2×10^{-6}	1.3
This work	8192	2	1	0.1222258910	M: 3.1×10^{-9}	**0 = ref**	

Note: The bold value indicates the best result of this work for $\psi_{\min}$.

Table 31 Results of the variables with extremes, Re = 7500, 8192 × 8192 grid

T	p_U	T_p(GCI)	$T_c(U_c)$	$\lvert T_c$-[6]$\rvert$	$\lvert T_c$-[18]$\rvert$	$\lvert T_c$-[12]$\rvert$
$u_{\min}$	1.998	-4.55037×10^{-1} (19)	$-4.55052229 \times 10^{-1}$ (17)	1.9×10^{-2}	6.3×10^{-3}	
$y(u_{\min})$	2.004	6.07416×10^{-2} (15)	$6.07404122 \times 10^{-2}$ (24)	1.8×10^{-3}	1.8×10^{-3}	
$v_{\min}$	1.999	-5.80430×10^{-1} (25)	$-5.80450027 \times 10^{-1}$ (13)	2.8×10^{-2}		
$x(v_{\min})$	2.008	9.6461837×10^{-1} (78)	$9.646189925 \times 10^{-1}$ (22)	3.7×10^{-3}		
$v_{\max}$	1.996	4.58345×10^{-1} (18)	$4.58359352 \times 10^{-1}$ (26)	1.9×10^{-2}	6.9×10^{-3}	
$x(v_{\max})$	1.996	6.66203×10^{-2} (12)	$6.66192818 \times 10^{-2}$ (16)	4.1×10^{-3}	2.2×10^{-4}	
$\psi_{\min}$	1.996	-1.223831×10^{-1} (44)	$-1.223866015 \times 10^{-1}$ (57)	2.4×10^{-3}	7.8×10^{-4}	6.3×10^{-6}
$x(\psi_{\min})$	2.057	5.1309736×10^{-1} (16)	$5.130974872 \times 10^{-1}$ (33)	1.4×10^{-3}	1.4×10^{-3}	1.2×10^{-4}
$y(\psi_{\min})$	2.015	5.3189221×10^{-1} (63)	$5.318917111 \times 10^{-1}$ (34)	3.1×10^{-4}	5.9×10^{-4}	2.0×10^{-4}

expected as the results reported in the literature were used in comparisons ranging from very coarse (11×11) to very fine (2048×2048) grids, as well as orders of accuracy (p_o) ranging from low (1), most common (2) to high (3, 5, 6, 7, 8, 10, and 160).

A total of 82 comparisons between U and D were made for the nine values of Reynolds number (as shown in Table 38), using the R ratio for the variable $\psi_{\min}$. U was calculated using at least five different procedures (A, B, C, O, and M). Nevertheless, $R < 1$ in

Table 32 Profile of u at $x = 1/2$, Re = 7500, and 8192 × 8192 grid

$u(y)$	p_U	T_h(GCI)	$T_c(U_c)$	$\lvert T_c$-[6]$\rvert$	$\lvert T_c$-[14]$\rvert$
$u(0.0546875)$	1.998	-4.51287×10^{-1} (21)	$-4.51303832 \times 10^{-1}$ (13)	2.0×10^{-2}	
$u(0.0625)$	1.998	-4.54759×10^{-1} (19)	$-4.54774105 \times 10^{-1}$ (16)	1.8×10^{-3}	
$u(0.0703125)$	1.997	-4.48068×10^{-1} (17)	$-4.48081043 \times 10^{-1}$ (18)	1.8×10^{-2}	
$u(0.1015625)$	1.996	-4.00136×10^{-1} (14)	$-4.00147265 \times 10^{-1}$ (19)	1.7×10^{-2}	
$u(0.125)$	1.996	-3.76379×10^{-1} (14)	$-3.76389729 \times 10^{-1}$ (18)		
$u(0.171875)$	1.996	-3.33445×10^{-1} (12)	$-3.33454158 \times 10^{-1}$ (16)	9.5×10^{-3}	
$u(0.1875)$	1.996	-3.18879×10^{-1} (11)	$-3.18887759 \times 10^{-1}$ (16)		
$u(0.25)$	1.996	-2.609314×10^{-1} (89)	$-2.60938576 \times 10^{-1}$ (14)		
$u(0.28125)$	1.996	-2.320269×10^{-1} (78)	$-2.32033186 \times 10^{-1}$ (13)	2.7×10^{-4}	
$u(0.3125)$	1.995	-2.031333×10^{-1} (68)	$-2.03138709 \times 10^{-1}$ (12)		
$u(0.375)$	1.995	-1.453313×10^{-1} (46)	$-1.453350005 \times 10^{-1}$ (94)		
$u(0.4375)$	1.992	-8.73688×10^{-2} (25)	$-8.73708560 \times 10^{-2}$ (71)		
$u(0.453125)$	1.991	-7.28206×10^{-2} (20)	$-7.28222323 \times 10^{-2}$ (65)	2.2×10^{-3}	
$u(0.5)$	1.972	-2.893091×10^{-2} (47)	$-2.89312795 \times 10^{-2}$ (49)	9.1×10^{-3}	2.3×10^{-4}
$u(0.5625)$	2.004	3.05095×10^{-2} (16)	$3.05108049 \times 10^{-2}$ (23)		
$u(0.6171875)$	2.000	8.39395×10^{-2} (35)	$8.3942277686 \times 10^{-2}$ (87)	5.2×10^{-4}	
$u(0.625)$	2.000	9.17203×10^{-2} (38)	$9.172332894 \times 10^{-2}$ (45)		
$u(0.6875)$	1.998	1.557406×10^{-1} (60)	$1.557453906 \times 10^{-1}$ (36)		
$u(0.734375)$	1.998	2.064095×10^{-1} (78)	$2.064156940 \times 10^{-1}$ (65)	5.1×10^{-4}	
$u(0.75)$	1.998	2.239427×10^{-1} (84)	$2.239494049 \times 10^{-1}$ (75)		
$u(0.8125)$	1.997	2.98159×10^{-1} (11)	$2.98167593 \times 10^{-1}$ (13)		
$u(0.8515625)$	1.997	3.48651×10^{-1} (13)	$3.48661598 \times 10^{-1}$ (16)	6.4×10^{-3}	
$u(0.875)$	1.996	3.80806×10^{-1} (14)	$3.80817201 \times 10^{-1}$ (19)		
$u(0.9375)$	1.996	4.74994×10^{-1} (18)	$4.75007939 \times 10^{-1}$ (27)		
$u(0.953125)$	1.996	4.90767×10^{-1} (19)	$4.90782762 \times 10^{-1}$ (30)	1.9×10^{-2}	
$u(0.9609375)$	1.996	4.92509×10^{-1} (20)	$4.92524988 \times 10^{-1}$ (32)	1.9×10^{-2}	
$u(0.96875)$	1.995	4.89181×10^{-1} (20)	$4.89196222 \times 10^{-1}$ (35)	1.9×10^{-2}	
$u(0.9765625)$	1.993	4.88566×10^{-1} (17)	$4.88579917 \times 10^{-1}$ (44)	1.6×10^{-2}	

Table 33 Profile of v at $y = 1/2$, Re = 7500, and 8192 × 8192 grid

$v(x)$	p_U	T_h(GCI)	$T_c(U_c)$	$\lvert T_c$-[6]$\rvert$	$\lvert T_c$-[14]$\rvert$
$v(0.0625)$	1.996	4.57391×10^{-1} (18)	$4.57406057 \times 10^{-1}$ (26)	1.9×10^{-2}	
$v(0.0703125)$	1.996	4.57656×10^{-1} (17)	$4.57670130 \times 10^{-1}$ (25)	1.7×10^{-2}	
$v(0.078125)$	1.996	4.52437×10^{-1} (16)	$4.52449565 \times 10^{-1}$ (23)	1.7×10^{-2}	
$v(0.09375)$	1.996	4.33598×10^{-1} (14)	$4.33609334 \times 10^{-1}$ (21)	1.5×10^{-2}	
$v(0.125)$	1.996	3.93576×10^{-1} (13)	$3.93586767 \times 10^{-1}$ (20)		
$v(0.15625)$	1.996	3.58938×10^{-1} (12)	$3.58947652 \times 10^{-1}$ (17)	8.3×10^{-3}	
$v(0.1875)$	1.996	3.25304×10^{-1} (11)	$3.25313031 \times 10^{-1}$ (15)		
$v(0.2265625)$	1.997	2.840871×10^{-1} (98)	$2.84094920 \times 10^{-1}$ (12)	2.9×10^{-3}	
$v(0.234375)$	1.997	2.759478×10^{-1} (95)	$2.75955461 \times 10^{-1}$ (12)	2.5×10^{-3}	
$v(0.25)$	1.997	2.597567×10^{-1} (90)	$2.59763868 \times 10^{-1}$ (11)		
$v(0.3125)$	1.997	1.959530×10^{-1} (69)	$1.959584475 \times 10^{-1}$ (65)		
$v(0.375)$	1.998	1.333213×10^{-1} (48)	$1.333250820 \times 10^{-1}$ (30)		
$v(0.4375)$	2.000	7.14523×10^{-2} (27)	$7.145443682 \times 10^{-2}$ (19)		
$v(0.5)$	2.012	9.88516×10^{-3} (67)	9.8856955×10^{-3} (30)	1.6×10^{-3}	1.4×10^{-5}
$v(0.5625)$	1.989	-5.19581×10^{-2} (14)	$-5.19592434 \times 10^{-2}$ (58)		
$v(0.625)$	1.994	-1.147738×10^{-1} (36)	$-1.147766552 \times 10^{-1}$ (83)		
$v(0.6875)$	1.995	-1.793515×10^{-1} (58)	$-1.79356084 \times 10^{-1}$ (11)		
$v(0.75)$	1.996	-2.465353×10^{-1} (82)	$-2.46541783 \times 10^{-1}$ (13)		
$v(0.8046875)$	1.996	-3.08117×10^{-1} (10)	$-3.08125079 \times 10^{-1}$ (15)	3.6×10^{-3}	
$v(0.8125)$	1.996	-3.17158×10^{-1} (11)	$-3.17166333 \times 10^{-1}$ (16)		
$v(0.859375)$	1.996	-3.72938×10^{-1} (13)	$-3.72948239 \times 10^{-1}$ (18)	1.1×10^{-2}	
$v(0.875)$	1.996	-3.92199×10^{-1} (13)	$-3.92209992 \times 10^{-1}$ (18)		
$v(0.90625)$	1.997	-4.29397×10^{-1} (16)	$-4.29409306 \times 10^{-1}$ (19)	1.9×10^{-2}	
$v(0.9375)$	1.995	-4.71935×10^{-1} (13)	$-4.71944892 \times 10^{-1}$ (25)		
$v(0.9453125)$	1.994	-4.99148×10^{-1} (12)	$-4.99156963 \times 10^{-1}$ (24)	1.3×10^{-2}	
$v(0.953125)$	1.996	-5.38262×10^{-1} (15)	$-5.38273506 \times 10^{-1}$ (22)	1.5×10^{-2}	
$v(0.9609375)$	1.998	-5.74393×10^{-1} (23)	$-5.74411336 \times 10^{-1}$ (17)	2.8×10^{-2}	
$v(0.96875)$	2.000	-5.70665×10^{-1} (30)	$-5.706897035 \times 10^{-1}$ (46)	3.2×10^{-2}	

only 15% of cases; hence, the estimated error (U) is lower than the deviation D for the best result herein. Moreover, in the other comparisons (85% of the cases), $1 \leq R < 10$, that is, the estimated error (U) is reliable and relatively accurate. This indicates that even the simplest procedure adopted here, GCI(p_o), can produce acceptable estimates of the discretization error.

The effect of the grid on the velocity profile of u at $x = 1/2$ and v at $y = 1/2$ for Re = 10,000 is shown in Figs. 5 and 6. The profiles of the nine coarsest grids (4 × 4 to 1024 × 1024) were partially or fully distinguishable. However, the profiles of the four finest grids (1024 × 1024 to 8192 × 8192) are superimposed, indicating a visual convergence of the solutions in relation to the discretization error.

Table 34 Comparisons of ψ_{min}, Re = 7500

Reference	Grid	p_o	RE	$-\psi_{min}$	U	D	R
[6]	257	2		0.119976		2.4×10^{-3}	
[14]	601	2		0.120924	C: 1.9×10^{-3}	1.5×10^{-3}	1.3
[18]	257	3		0.121605	B: 1.9×10^{-3}	7.8×10^{-4}	2.4
[10]	256	1		0.1217		6.9×10^{-4}	
[17]	1025	2		0.121939		4.5×10^{-4}	
This work	2048	2		0.122331		5.6×10^{-5}	
This work	4096	2		0.122373	B: 4.2×10^{-5}	1.4×10^{-5}	3.0
[12]	257	8		0.1223803	A: 1×10^{-5}	6.3×10^{-6}	1.6
This work	8192	2		0.1223831	C: 4.4×10^{-6}	3.5×10^{-6}	1.3
[14]	601	2	2	0.122386		6.0×10^{-7}	
This work	8192	2	1	0.1223866015	M: 5.7×10^{-9}	**0 = ref**	

Note: The bold value indicates the best result of this work for ψ_{min}.

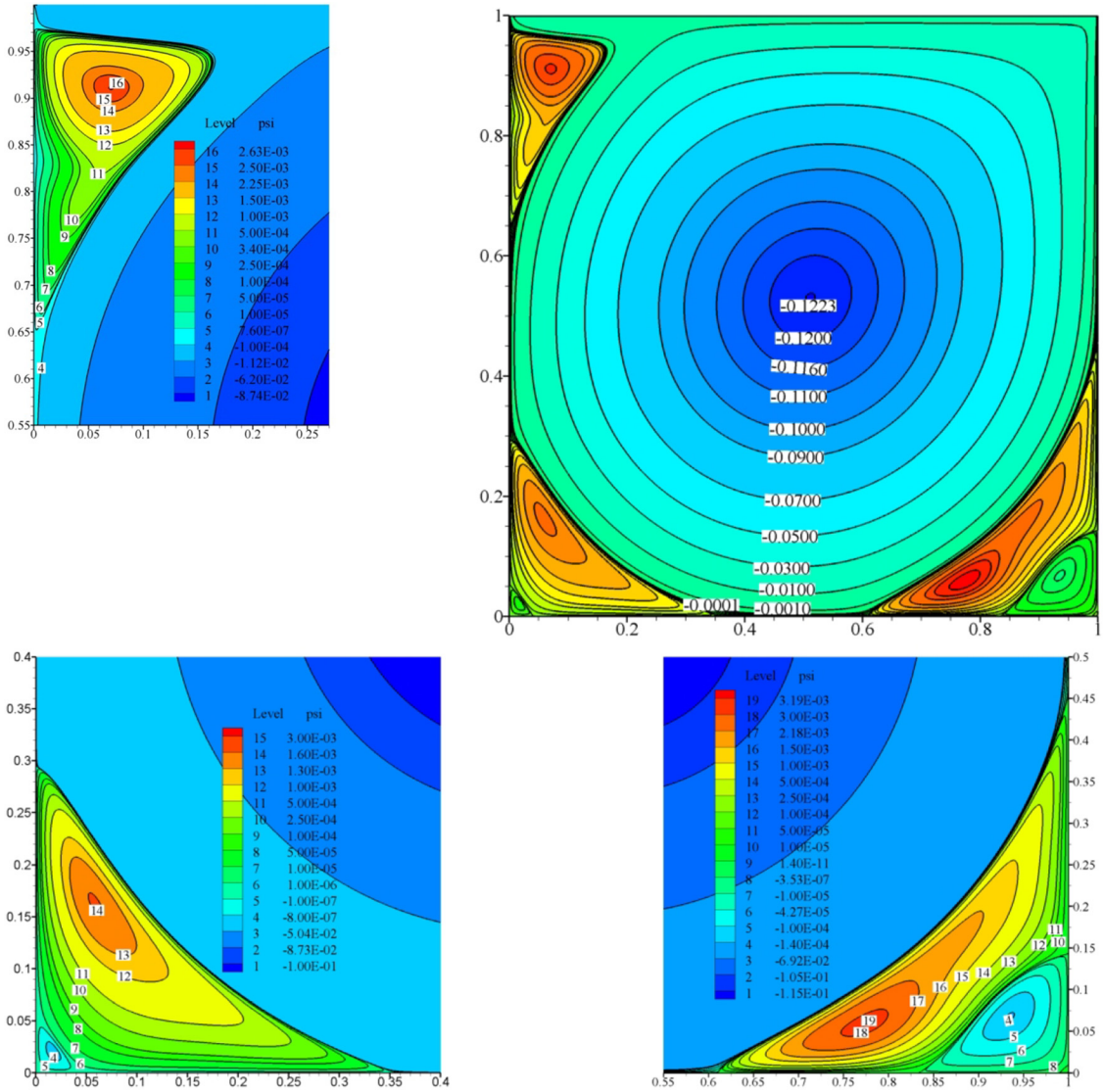

Fig. 3 Streamline contours, Re = 10,000, 2048 × 2048 grid

In general, the number of significant digits in the solutions of T_h and T_p decreases as the Reynolds number increases from 8 to 12 digits in Re = 1 down to 5 to 8 digits at Re = 10,000. The same applies to the solutions of T_c, which range from 10 to 13 digits in Re = 1 down to 8 to 10 digits at Re = 10,000. Therefore, using the convergent solution (T_c) is important because with a simple extrapolation procedure, the discretization error can be reduced by two or three significant digits of the T_h and T_p solutions, regardless of the Reynolds number. This variation in the number of digits for the same Reynolds number is due to the different types of variables of interest, which are affected differently by grid refinement, which is the basis for calculating error estimates.

The 585 T_c results fall within the range of $T_h \pm$ GCI or $T_p \pm$ GCI, as appropriate. This indicates coherence between the

Table 35 Results of the variables with extremes, Re = 10,000, 8192 × 8192 grid

T	p_U	T_p(GCI)	$T_c(U_c)$	$\lvert T_c$-[6]$\rvert$	$\lvert T_c$-[17]$\rvert$	$\lvert T_c$-[12]$\rvert$
$u_{\min}$	1.993	-4.59049×10^{-1} (27)	$-4.59070247 \times 10^{-1}$ (66)	3.2×10^{-2}		
$y(u_{\min})$	1.992	5.28105×10^{-2} (20)	$5.28088974 \times 10^{-2}$ (58)	1.9×10^{-3}		
$v_{\min}$	1.993	-5.82169×10^{-1} (35)	$-5.82196556 \times 10^{-1}$ (89)	3.9×10^{-2}		
$x(v_{\min})$	1.990	9.688732×10^{-1} (11)	$9.688740317 \times 10^{-1}$ (39)	1.2×10^{-4}		
$v_{\max}$	1.993	4.64899×10^{-1} (24)	$4.64918302 \times 10^{-1}$ (59)	2.5×10^{-2}		
$x(v_{\max})$	1.994	5.85953×10^{-2} (15)	$5.85940570 \times 10^{-2}$ (35)	3.9×10^{-3}		
$\psi_{\min}$	1.993	-1.223946×10^{-1} (61)	$-1.22399499 \times 10^{-1}$ (15)	2.7×10^{-3}	6.2×10^{-4}	6.5×10^{-6}
$x(\psi_{\min})$	1.992	5.1190289×10^{-1} (35)	$5.119031767 \times 10^{-1}$ (11)	2.0×10^{-4}	2.0×10^{-4}	5.7×10^{-4}
$y(\psi_{\min})$	1.991	5.3002583×10^{-1} (85)	$5.300251601 \times 10^{-1}$ (28)	3.3×10^{-3}	2.7×10^{-4}	1.8×10^{-4}

Table 36 Profile of u at $x = 1/2$, Re = 10,000, and 8192 × 8192 grid

$u(y)$	p_U	T_h(GCI)	$T_c(U_c)$	$\lvert T_c$-[6]$\rvert$	$\lvert T_c$-[14]$\rvert$
$u(0.0546875)$	1.994	-4.58650×10^{-1} (27)	$-4.58671564 \times 10^{-1}$ (60)	3.1×10^{-2}	
$u(0.0625)$	1.994	-4.50416×10^{-1} (23)	$-4.50434272 \times 10^{-1}$ (50)	2.5×10^{-2}	
$u(0.0703125)$	1.994	-4.36896×10^{-1} (21)	$-4.36912169 \times 10^{-1}$ (45)	2.0×10^{-2}	
$u(0.1015625)$	1.994	-3.94667×10^{-1} (20)	$-3.94682887 \times 10^{-1}$ (46)	1.5×10^{-2}	
$u(0.125)$	1.994	-3.73661×10^{-1} (19)	$-3.73675860 \times 10^{-1}$ (43)		
$u(0.171875)$	1.994	-3.30453×10^{-1} (16)	$-3.30465541 \times 10^{-1}$ (37)	3.4×10^{-3}	
$u(0.1875)$	1.994	-3.16052×10^{-1} (15)	$-3.16064831 \times 10^{-1}$ (35)		
$u(0.25)$	1.994	-2.58556×10^{-1} (12)	$-2.58566309 \times 10^{-1}$ (28)		
$u(0.28125)$	1.994	-2.29796×10^{-1} (11)	$-2.29805029 \times 10^{-1}$ (24)	2.1×10^{-3}	
$u(0.3125)$	1.994	-2.010184×10^{-1} (93)	$-2.01025842 \times 10^{-1}$ (21)		
$u(0.375)$	1.994	-1.433855×10^{-1} (63)	$-1.43390600 \times 10^{-1}$ (14)		
$u(0.4375)$	1.994	-8.55406×10^{-2} (34)	$-8.55433540 \times 10^{-2}$ (70)		
$u(0.453125)$	1.995	-7.10173×10^{-2} (27)	$-7.10194900 \times 10^{-2}$ (54)	4.4×10^{-3}	
$u(0.5)$	1.999	-2.719905×10^{-2} (56)	$-2.719950155 \times 10^{-2}$ (28)	3.9×10^{-3}	4.0×10^{-4}
$u(0.5625)$	1.992	3.21351×10^{-2} (23)	$3.21369270 \times 10^{-2}$ (66)		
$u(0.6171875)$	1.993	8.54356×10^{-2} (49)	8.5439567×10^{-2} (13)	2.0×10^{-3}	
$u(0.625)$	1.993	9.31935×10^{-2} (53)	9.3197744×10^{-2} (14)		
$u(0.6875)$	1.993	1.569730×10^{-1} (84)	$1.56979703 \times 10^{-1}$ (21)		
$u(0.734375)$	1.993	2.07376×10^{-1} (11)	$2.07384526 \times 10^{-1}$ (27)	6.5×10^{-4}	
$u(0.75)$	1.993	2.24801×10^{-1} (12)	$2.24810058 \times 10^{-1}$ (29)		
$u(0.8125)$	1.993	2.98475×10^{-1} (15)	$2.98487063 \times 10^{-1}$ (38)		
$u(0.8515625)$	1.993	3.48565×10^{-1} (18)	$3.48579444 \times 10^{-1}$ (43)	2.2×10^{-3}	
$u(0.875)$	1.993	3.80475×10^{-1} (19)	$3.80490013 \times 10^{-1}$ (47)		
$u(0.9375)$	1.993	4.75279×10^{-1} (24)	$4.75298700 \times 10^{-1}$ (58)		
$u(0.953125)$	1.994	4.96030×10^{-1} (26)	$4.96050898 \times 10^{-1}$ (63)	1.8×10^{-2}	
$u(0.9609375)$	1.994	5.00884×10^{-1} (27)	$5.00906073 \times 10^{-1}$ (64)	2.0×10^{-2}	
$u(0.96875)$	1.994	4.99261×10^{-1} (28)	$4.99283237 \times 10^{-1}$ (65)	2.1×10^{-2}	
$u(0.9765625)$	1.994	4.92467×10^{-1} (26)	$4.92487682 \times 10^{-1}$ (62)	2.0×10^{-2}	

Table 37 Profile of v at $y = 1/2$, Re = 10,000, and 8192 × 8192 grid

$v(x)$	p_U	T_h(GCI)	$T_c(U_c)$	$\lvert T_c$-[6]$\rvert$	$\lvert T_c$-[14]$\rvert$
$v(0.0625)$	1.994	4.63954×10^{-1} (24)	$4.63972755 \times 10^{-1}$ (56)	2.4×10^{-2}	
$v(0.0703125)$	1.994	4.57618×10^{-1} (22)	$4.57635785 \times 10^{-1}$ (52)	2.0×10^{-2}	
$v(0.078125)$	1.994	4.47860×10^{-1} (21)	$4.47877085 \times 10^{-1}$ (49)	1.7×10^{-2}	
$v(0.09375)$	1.994	4.26267×10^{-1} (20)	$4.26282518 \times 10^{-1}$ (47)	1.1×10^{-2}	
$v(0.125)$	1.994	3.89165×10^{-1} (19)	$3.89179496 \times 10^{-1}$ (44)		
$v(0.15625)$	1.994	3.55064×10^{-1} (17)	$3.55077123 \times 10^{-1}$ (40)	4.4×10^{-3}	
$v(0.1875)$	1.994	3.21681×10^{-1} (15)	$3.21693329 \times 10^{-1}$ (37)		
$v(0.2265625)$	1.994	2.80897×10^{-1} (14)	$2.80907839 \times 10^{-1}$ (32)	8.8×10^{-4}	
$v(0.234375)$	1.994	2.72838×10^{-1} (13)	$2.72848325 \times 10^{-1}$ (31)	6.1×10^{-4}	
$v(0.25)$	1.994	2.56801×10^{-1} (12)	$2.56810950 \times 10^{-1}$ (30)		
$v(0.3125)$	1.994	1.935534×10^{-1} (96)	$1.93561088 \times 10^{-1}$ (23)		
$v(0.375)$	1.993	1.313924×10^{-1} (67)	$1.31397724 \times 10^{-1}$ (16)		
$v(0.4375)$	1.993	6.99357×10^{-2} (39)	$6.99387588 \times 10^{-2}$ (94)		
$v(0.5)$	1.993	8.7566×10^{-3} (10)	8.7574246×10^{-3} (27)	4.5×10^{-4}	4.3×10^{-5}
$v(0.5625)$	1.994	-5.26887×10^{-2} (19)	$-5.26901620 \times 10^{-2}$ (42)		
$v(0.625)$	1.994	-1.150658×10^{-1} (49)	$-1.15069698 \times 10^{-1}$ (11)		
$v(0.6875)$	1.994	-1.791377×10^{-1} (80)	$-1.79144111 \times 10^{-1}$ (19)		
$v(0.75)$	1.994	-2.45722×10^{-1} (11)	$-2.45730732 \times 10^{-1}$ (27)		
$v(0.8046875)$	1.994	-3.06676×10^{-1} (14)	$-3.06687583 \times 10^{-1}$ (34)	5.0×10^{-4}	
$v(0.8125)$	1.994	-3.15619×10^{-1} (15)	$-3.15631301 \times 10^{-1}$ (35)		
$v(0.859375)$	1.994	-3.70627×10^{-1} (18)	$-3.70641458 \times 10^{-1}$ (42)	3.3×10^{-3}	
$v(0.875)$	1.994	-3.89570×10^{-1} (19)	$-3.89585408 \times 10^{-1}$ (44)		

Table 37 (continued)

$v(x)$	p_U	T_h(GCI)	$T_c(U_c)$	$\lvert T_c$-[6]$\rvert$	$\lvert T_c$-[14]$\rvert$
$v(0.90625)$	1.994	-4.28012×10^{-1} (21)	$-4.28029389 \times 10^{-1}$ (50)	1.3×10^{-2}	
$v(0.9375)$	1.993	-4.62067×10^{-1} (21)	$-4.62084440 \times 10^{-1}$ (56)		
$v(0.9453125)$	1.993	-4.77944×10^{-1} (18)	$-4.77958012 \times 10^{-1}$ (46)	1.9×10^{-2}	
$v(0.953125)$	1.994	-5.08390×10^{-1} (16)	$-5.08402758 \times 10^{-1}$ (33)	1.7×10^{-2}	
$v(0.9609375)$	1.995	-5.53115×10^{-1} (23)	$-5.53133348 \times 10^{-1}$ (41)	2.3×10^{-2}	
$v(0.96875)$	1.994	-5.82156×10^{-1} (38)	$-5.82186386 \times 10^{-1}$ (85)	3.9×10^{-2}	

Table 38 Comparisons of ψ_{min}, Re = 10,000

Reference	Grid	p_o	RE	$-\psi_{min}$	U	D	R
[4]	51	1		0.0873		3.5×10^{-2}	
This work	128	2	1	0.153	M: 3.8×10^{-2}	3.1×10^{-2}	1.2
[7]	180	2		0.10284	C: 3.7×10^{-2}	2.0×10^{-2}	1.9
This work	128	2		0.11	C: 1.0×10^{-1}	1.2×10^{-2}	8.3
This work	256	2		0.118	C: 1.2×10^{-2}	4.4×10^{-3}	2.7
[7]	180	2	3	0.12522		2.8×10^{-3}	
[6]	257	2		0.119731		2.7×10^{-3}	
This work	256	2	1	0.1244	M: 3.1×10^{-3}	2.0×10^{-3}	1.6
[14]	601	2		0.120403	C: 2.6×10^{-3}	2.0×10^{-3}	1.3
[5]	151	2		0.1211	C: 1.2×10^{-4}	1.3×10^{-3}	0.09
This work	512	2		0.1212	C: 1.8×10^{-3}	1.2×10^{-3}	1.5
[5]	151	2	1	0.1212		1.2×10^{-3}	
[17]	1025	2		0.121781		6.2×10^{-4}	
This work	1024	2		0.12209	C: 4.3×10^{-4}	3.1×10^{-4}	1.4
This work	2048	2		0.12232	C: 1.0×10^{-4}	7.9×10^{-5}	1.3
This work	512	2	1	0.12245	M: 2.0×10^{-4}	5.1×10^{-5}	3.9
This work	4096	2		0.122380	C: 2.5×10^{-5}	1.9×10^{-5}	1.3
[14]	601	2	2	0.122390		9.5×10^{-6}	
This work	1024	2	1	0.122408	M: 2.7×10^{-5}	8.5×10^{-6}	3.2
[12]	257	8		0.1223930	A: 1×10^{-5}	6.5×10^{-6}	1.5
This work	8192	2		0.1223946	C: 6.1×10^{-6}	4.9×10^{-6}	1.2
This work	2048	2	1	0.1224007	M: 3.0×10^{-6}	1.2×10^{-6}	2.5
This work	4096	2	1	0.12239969	M: 2.9×10^{-7}	1.9×10^{-7}	1.5
This work	8192	2	9	0.122399489	O: 3.3×10^{-8}	1.0×10^{-8}	3.3
This work	8192	2	1	0.122399499	M: 1.5×10^{-8}	**0 = ref**	

Note: The bold value indicates the best result of this work for ψ_{min}.

extrapolated (T_c) and nonextrapolated (T_h or T_p) results, as all numerical results tend toward the analytical solution of the problem. This also increases the reliability of the numerical results.

4.11 Upper Left Secondary Vortex. The appearance of the upper left secondary vortex (Fig. 3) was estimated to occur at Re = 1200 [5] and 1500 [8]. Streamlines are shown in Fig. 7 in the region of the upper left secondary vortex for six values of Reynolds number. These results were obtained using a grid of 2048 × 2048 volumes. The vortex is present at Re = 1400 but is small; it can be verified based on the values of the stream function field (not mentioned here). At Re = 1425, the vortex is already well characterized and increases in size as the Reynolds number increases. The vortex was not present at Re = 1380, and we did not test other Reynolds numbers between 1380 and 1400.

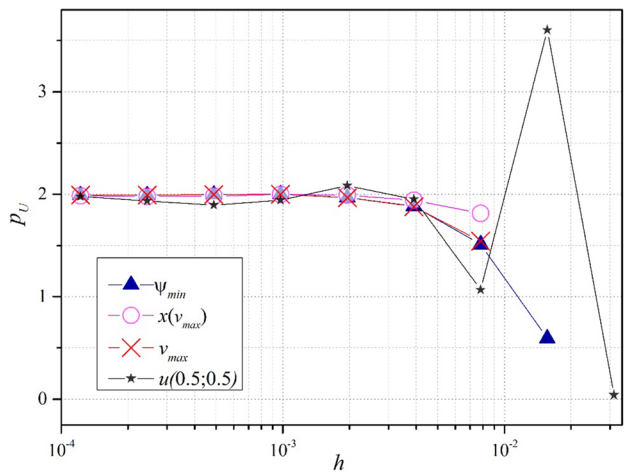

Fig. 4 Equivalent apparent order (p_U) for four variables and Re = 1000

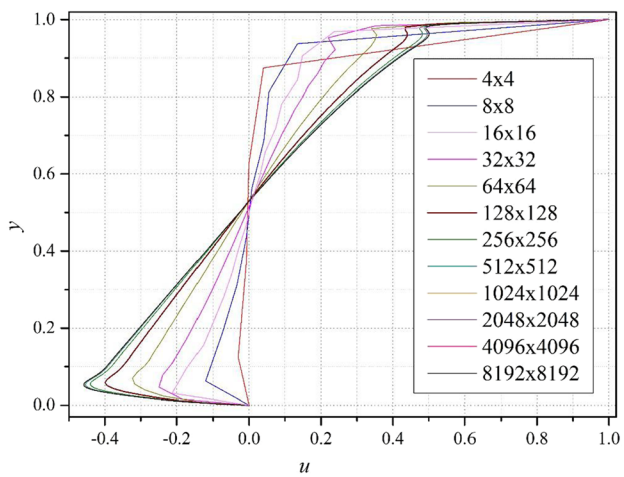

Fig. 5 Velocity profile of u at $x = 1/2$ for Re = 10,000

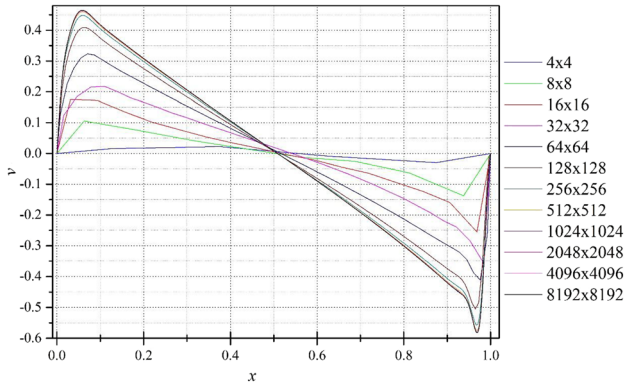

Fig. 6 Velocity profile of v at $y = 1/2$ for Re = 10,000

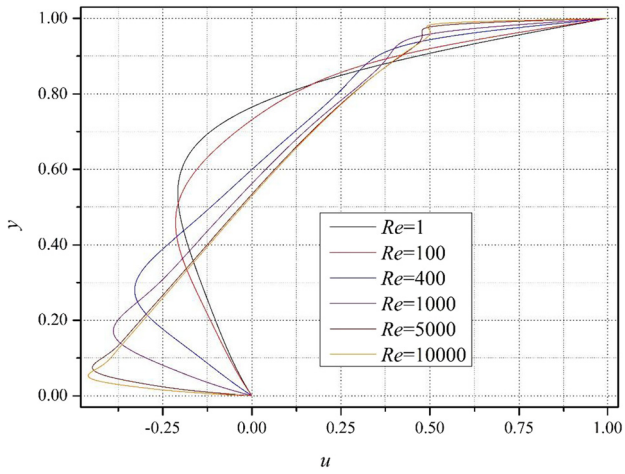

Fig. 8 Velocity profile of u at $x = 1/2$ and 8192 × 8192 grid

4.12 Functions of Re. The behavior of the velocity profiles of u at $x = 1/2$ is shown in Fig. 8 for six values of the Reynolds number. The velocity profiles of v at $y = 1/2$ are shown in Fig. 9. The results were obtained using a grid of 8192×8192 volumes. The profiles of $\mathrm{Re} = 10$, not shown here, were visually coincident with $\mathrm{Re} = 1$. The behavior of the profiles differs significantly depending on the Reynolds number and can be divided into three intervals. Up to $\mathrm{Re} = 100$, the variations between the two walls were smooth and monotonic. For $\mathrm{Re} \geq 5000$, the region of transition between the boundary layers of the two walls is quite distinct, with minimal locations in the profiles of u on the upper wall, and an almost linear variation of the profile between the two boundary layers. The vortex core is not yet in perfect solid body rotation, which is theoretically expected for asymptotically large Reynolds numbers. Finally, for $\mathrm{Re} = 400$ and 1000, the behavior is intermediate between the two previous intervals.

The variation of $\psi_{\min}$ and its coordinates for 39 Reynolds numbers between 0 and 10,000 are shown in Table 39. The results reported in the literature and their differences (D) from the present work are presented together. The bold values indicate the local or global minima and maxima for each variable. The results presented herein were obtained on a grid of 8192×8192 volumes without interpolation, that is, T_h, as described in Sec. 3. The estimated discretization error falls within the order of the last digit presented in each result, which is sufficient to demonstrate the behavior of $\psi_{\min}$ and its coordinates with the Reynolds number. $\psi_{\min}$ and $y(\psi_{\min})$ decrease monotonically in response to an increase in the Reynolds number. On the contrary, $x(\psi_{\min})$ increases with the increase in Reynolds number up to $\mathrm{Re} = 150$, where it reaches its maximum global value, after which its value decreases monotonically with an increase in the Reynolds number. Therefore, the results of this study, with a much larger grid than those previously reported in the literature, are in agreement with previous studies [5,9–11,19,21,22], which show that the minimum value of the stream function always decreases with the increase in Reynolds number and is not compatible with the

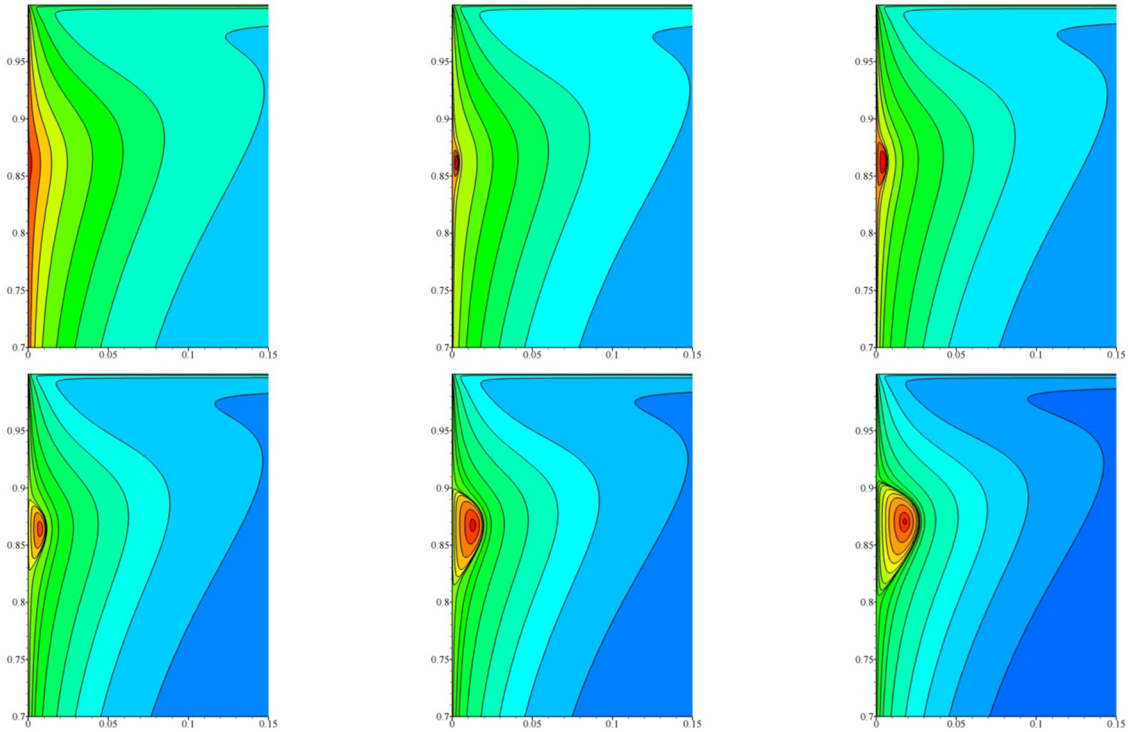

Fig. 7 Streamline contours in the region of the upper left secondary vortex for Re = 1400, 1425, 1450, 1500, 1600, and 1700; 2048 × 2048 grid

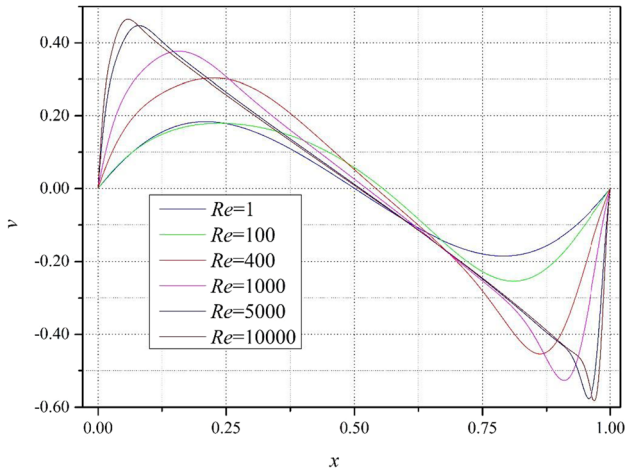

Fig. 9 Velocity profile of v at $y = 1/2$ and 8192×8192 grid

results reported in other studies [1,2,4,6–8,12,14,17,18], which demonstrate a different behavior.

The variation in velocity with extremes and their coordinates for 38 values of Reynolds numbers between 0.0001 and 10,000 are shown in Table 40. The results of $u(0.5, 0.5)$ and $v(0.5; 0.5)$ are also presented. The bold values indicate the local or global minima and maxima for each variable. The results were obtained with a grid of 8192×8192 volumes without interpolation, that is, T_h, as described in Sec. 3. The estimated discretization error is in the order of the last digit presented in each result, which is sufficient to demonstrate the behavior of the variables with the Reynolds number. As can be seen, $y(u_{\min})$ and $v_{\min}$ decrease monotonically with an increase in the Reynolds number. Conversely, $x(v_{\min})$ increases monotonically with an increase in the Reynolds number. The variables $u_{\min}$, $v(0.5, 0.5)$, and $x(v_{\max})$ increase with the increase in the Reynolds number up to $\mathrm{Re} = 40$, 200, and 200, respectively, when they reach their global maximum values; thereafter, their values decrease monotonically with the increase in the Reynolds number. The variable $v_{\max}$ decreases with an increase in the Reynolds number up to $\mathrm{Re} = 64$, when it reaches its global minimum value, after which its value increases monotonically with the increase in the Reynolds number. The variable $u(0.5, 0.5)$ presents the most complex behavior: initially, its value increases with the increase in the Reynolds number until it reaches a local maximum at $\mathrm{Re} = 35$; its value then decreases with the increase in the Reynolds number until it reaches its global minimum at $\mathrm{Re} = 150$, whereupon its value increases monotonically with the increase in the Reynolds number.

The size of the secondary vortices for nine values of Reynolds number is shown in Table 41, where VS denotes the number of secondary vortices, BL is the lower left vortex, BR is the lower right vortex, and TL is the upper left vortex; X and Y indicate the dimensions of the vortices in the x- and y-directions, respectively. The size was measured from the corner to the wall separation point, regardless of the presence of tertiary vortices. The bold

Table 39 $\psi_{\min}$ and its coordinates for 39 values of Re; 8192×8192 grid

Re	Reference	Grid	p_o	RE	$\psi_{\min}$	$\psi_{\min}$	$x(\psi_{\min})$	$y(\psi_{\min})$	D
0	[13]	49	48		−0.10007627				
0.0001	[12]	32	8		−0.1000758	**−0.10007626**	**0.50000**	**0.76501**	4.6×10^{-7}
0.001						**−0.10007626**	**0.50000**	**0.76501**	
0.01	[16]	1024	2	9	−0.10007622	**−0.10007626**	**0.50000**	**0.76501**	4×10^{-8}
0.1						**−0.10007626**	0.50012	**0.76501**	
1	[12]	5	6		−0.10005	−0.10007662	0.50171	**0.76501**	2.7×10^{-5}
2						−0.10007771	0.50330	**0.76501**	
4						−0.10008209	0.50671	**0.76501**	
8	[1]	11	2		−0.09	−0.10009959	0.51331	0.76489	1.0×10^{-2}
10	[2]	41	2		−0.1000	−0.10011273	0.51660	0.76477	1.1×10^{-4}
16						−0.10016982	0.52649	0.76453	
32						−0.10045309	0.55151	0.76282	
35						−0.10052762	0.55591	0.76233	
40						−0.10066679	0.56299	0.76135	
64	[1]	11	2		−0.08	−0.10158256	0.59180	0.75488	2.2×10^{-2}
70						−0.10186863	0.59741	0.75256	
82						−0.10249379	0.60669	0.74719	
100	[3]	128	2		−0.1034	−0.10352093	0.61572	0.73730	1.2×10^{-4}
150						−0.1063908	**0.61682**	0.70166	
160						−0.1069092	0.61426	0.69421	
190						−0.1083149	0.60437	0.67322	
200	[2]	41	2		−0.1032	−0.1087355	0.60071	0.66699	5.5×10^{-3}
220						−0.1095117	0.59351	0.65576	
300						−0.1119368	0.57019	0.62500	
400	[6]	257	2		−0.113909	−0.1139888	0.55408	0.60547	8.0×10^{-5}
700	[4]	51	1		−0.0986	−0.1173067	0.53760	0.57861	1.9×10^{-2}
1000	[3]	65	2		−0.114	−0.1189362	0.53076	0.56519	4.9×10^{-3}
1400						−0.120128	0.52576	0.55554	
1500						−0.120332	0.52490	0.55396	
1700						−0.120670	0.52344	0.55115	
2000	[8]	321	1		−0.1116	−0.121048	0.52185	0.54785	9.5×10^{-3}
2500	[12]	257	8		−0.1214621	−0.121468	0.51978	0.54395	5.9×10^{-6}
3200	[5]	101	2	1	−0.1217	−0.121819	0.51782	0.54028	1.2×10^{-4}
4000	[7]	161	2	2	−0.12238	−0.122055	0.51636	0.53760	3.3×10^{-4}
5000	[6]	257	2		−0.118966	−0.122224	0.51514	0.53528	3.3×10^{-3}
5500						−0.122278	0.51465	0.53442	
6000						−0.122318	0.51416	0.53357	
7500	[14]	601	2	2	−0.122386	−0.122383	0.51306	0.53186	3×10^{-6}
10,000	[12]	257	8		−0.1223930	**−0.122395**	**0.51196**	**0.53003**	2×10^{-6}

Note: The bold values indicate the local or global minima and maxima for each variable.

Table 40 Velocity with extremes and their coordinates for 38 values of Re; 8192 × 8192 grid

Re	$u(0.5; 0.5)$	u_{min}	$y(u_{min})$	$v(0.5; 0.5)$	v_{min}	$x(v_{min})$	v_{max}	$x(v_{max})$
0.0001	**−0.20519168**	**−0.20775589**	**0.53595**	**0.0000000637**	**−0.18444494**	**0.79047**	**0.18444487**	**0.20953**
0.001	**−0.20519168**	**−0.20775589**	**0.53595**	0.0000006368	−0.18444529	**0.79047**	0.18444453	**0.20953**
0.01	**−0.20519168**	**−0.20775589**	**0.53595**	0.0000063677	−0.18444870	**0.79047**	0.18444111	**0.20953**
0.1	−0.20519167	−0.20775587	**0.53595**	0.0000636771	−0.18448291	0.79059	0.18440696	**0.20953**
1	−0.20519140	−0.20775405	**0.53595**	0.0006367636	−0.18482730	0.79083	0.18406777	0.20978
2	−0.20519055	−0.20774855	0.53583	0.001273483	−0.18521495	0.79108	0.18369589	0.21002
4	−0.20518719	−0.20772662	0.53571	0.002546614	−0.18600597	0.79169	0.18296792	0.21063
8	−0.20517413	−0.20764003	0.53522	0.005090409	−0.18765133	0.79279	0.18157556	0.21173
10	−0.20516470	−0.20757626	0.53485	0.006360366	−0.18850589	0.79327	0.18091152	0.21234
16	−0.2051275	−0.2073114	0.53314	0.010158211	−0.19119932	0.79486	0.17905093	0.21405
32	−0.2050288	−0.2062728	0.52484	0.020135458	−0.19938811	0.79889	0.17512313	0.21869
35	**−0.2050248**	−0.2060707	0.52264	0.021971748	−0.20109803	0.79950	0.17456868	0.21954
40	−0.2050401	**−0.2057665**	0.51886	0.025001906	−0.20407909	0.80072	0.17378329	0.22101
64	−0.2057509	−0.2057899	0.49579	0.038920327	−0.22085014	0.80524	**0.17265059**	0.22760
70	−0.2061430	−0.2063993	0.48944	0.042220727	−0.22571212	0.80621	0.17309201	0.22919
82	−0.2071851	−0.2085345	0.47662	0.048593099	−0.23623348	0.80804	0.17485506	0.23236
100	−0.2091490	−0.2140423	0.45807	0.057536573	−0.25380293	0.81049	0.17957277	0.23700
150	**−0.2108331**	−0.2390463	0.41388	0.0767420	−0.3077036	0.81720	0.2019549	0.24933
160	−0.2095262	−0.2446638	0.40619	0.0791939	−0.3181576	0.81879	0.2073003	0.25140
190	−0.2017326	−0.2608913	0.38458	0.0833162	−0.3469576	0.82416	0.2235838	0.25543
200	−0.1980187	−0.2659297	0.37799	**0.0836634**	−0.3555818	0.82611	0.2289092	**0.25592**
220	−0.1894020	−0.2753277	0.36517	0.0830394	−0.3713534	0.83002	0.2391879	0.25568
300	−0.1505924	−0.3045965	0.32135	0.0702711	−0.4182252	0.84576	0.2737233	0.24481
400	−0.1150536	−0.3287296	0.27997	0.0520582	−0.4540648	0.86224	0.3038321	0.22528
700	−0.0764255	−0.367962	0.20831	0.0318129	−0.504689	0.89264	0.352314	0.18243
1000	−0.0620560	−0.388568	0.17169	0.0257995	−0.527075	0.90924	0.376943	0.15778
1400	−0.0519855	−0.405242	0.14325	0.0213385	−0.54320	0.92267	0.396571	0.13727
1500	−0.0502799	−0.408343	0.13812	0.0205648	−0.54602	0.92511	0.400211	0.13336
1700	−0.0474425	−0.413701	0.12933	0.0192694	−0.55075	0.92950	0.406503	0.12665
2000	−0.0441881	−0.420158	0.11871	0.0177662	−0.55622	0.93475	0.414111	0.11823
2500	−0.0403803	−0.428148	0.10577	0.0159681	−0.56264	0.94122	0.423609	0.10760
3200	−0.0368976	−0.435896	0.09308	0.0142618	−0.56845	0.94769	0.432999	0.09674
4000	−0.0342856	−0.44200	0.08319	0.0129202	−0.57271	0.95282	0.44061	0.08783
5000	−0.0320884	−0.44730	0.07428	0.0117323	−0.57612	0.95746	0.44750	0.07965
5500	−0.0312578	−0.44934	0.07086	0.0112653	−0.57735	0.95929	0.45023	0.07648
6000	−0.0305497	−0.45108	0.06781	0.0108579	−0.57835	0.96088	0.45263	0.07355
7500	−0.0289309	−0.45504	0.06073	0.0098852	−0.58043	0.96466	0.45835	0.06659
10,000	**−0.0271991**	**−0.45905**	**0.05280**	**0.008757**	**−0.58217**	**0.96893**	**0.46490**	**0.05865**

Note: The bold values indicate the local or global minima and maxima for each variable.

Table 41 Size of the secondary vortices for nine values of Re; 2048 × 2048 grid

Re	VS	BL-*X*	BR-*X*	TL-*X*	BL-*Y*	BR-*Y*	TL-*Y*
1	2	**0.0917**	**0.0920**	**0**	**0.0932**	**0.0938**	**0**
10	2	0.0902	0.0939	0	0.0915	0.0961	0
100	2	**0.0845**	0.1375	0	**0.0838**	0.1557	0
400	2	0.1311	0.2647	0	0.1113	0.3261	0
1000	2	0.2274	0.3034	0	0.1716	0.3661	0
3200	3	0.3099	0.3479	0.0892	0.2481	0.4126	0.2278
5000	3	0.3293	0.3631	0.1204	0.2690	0.4242	0.2720
7500	3	0.3479	0.3796	0.1469	0.2846	0.4421	0.3100
10,000	3	**0.3558**	**0.3901**	**0.1638**	**0.2948**	**0.4500**	**0.3320**

Note: The bold values indicate the local or global minima and maxima for each variable.

values indicate the local or global minima and maxima for each vortex. The results were obtained using a grid of 2048 × 2048 volumes. The accuracy is not very good, but it is sufficient to illustrate how the dimensions of the vortices vary with the Reynolds number. The size of the BR, in both the *x*- and *y*-directions, always increases with the increase in Reynolds number; the same applies to the TL when it is present. However, BL, in both the *x*- and *y*-directions, initially decreases in size from Re = 1 to 100, where it reaches its smallest size, confirming the qualitative results reported by Burggraf [2]. Starting from Re = 100, BL exhibits the same behavior as the other vortices, that is, its size increases in response to the increase in Reynolds number.

5 Conclusion

Based on the results and analyses presented herein, we believe that our work provides the most accurate results in the current literature for the problem of laminar flow inside a square cavity with a lid in motion, for Re = 1, 10, 100, 400, 1000, 3200, 5000, 7500, and 10,000 of 65 variables of interest involving velocity profiles, their minimum and maximum values and their coordinates, and the minimum value of the stream function and its coordinates. In this paper, we presented 585 results without extrapolations, with equivalent apparent orders and estimated discretization errors. A further 585 results were also presented with extrapolations and their estimated discretization errors. Several of these results were compared with those of other studies available in the literature.

The variations of 11 selected variables are shown, with 38 values of Reynolds number between 0.0001 and 10,000, indicating that the behavior of some variables is not monotonic with the Reynolds number, a fact that has not yet been described in the literature. The results of this study, wherein we used a much larger grid than those reported in the literature, are in agreement with those of previous studies [5,9–11,19,21,22], demonstrating that the minimum value of the stream function always decreases with an increase in the Reynolds number.

It was verified with a 2048 × 2048 grid that the upper secondary vortex already exists at Re = 1400 and does not exist at Re = 1380; therefore, its appearance must be between these two

values. The size of the lower left vortex decreases from Re = 1 to 100, when it reaches its smallest size, and that starting from Re = 100, it exhibits the same behavior as the other secondary vortices; in other words, its size increases in response to the increase in Reynolds number.

Acknowledgment

We are especially grateful to Dr. Milovan Peric for making his code available on FORTRAN 77 which was used as the basis for this work.

The authors acknowledge the Department of Mechanical Engineering of Federal University of Paraná (UFPR), the Federal University of Technology—Paraná (UTFPR) in Apucarana, the UNIESPAÇO program of the Brazilian Space Agency (AEB), and the Conselho Nacional de Desenvolvimento Científico e Tecnológico (CNPq), Brazil, for physical and financial support given for this work. This study was financed in part by the Coordenação de Aperfeiçoamento de Pessoal de Nível Superior (CAPES), Brazil, Finance Code 001.

Cosmo D. Santiago and Carlos A. R. Carvalho, Jr. thank supported by CAPES scholarships. Carlos H. Marchi is supported by a CNPq scholarship.

We are grateful to all four reviewers and the Associate Editor for their comments and suggestions.

To all researchers who have already dedicated themselves to solving this problem and improving its results to serve as a test problem for many other researchers.

Funding Data

- Coordenação de Aperfeiçoamento de Pessoal de Nível Superior (CAPES), Brazil, Finance Code 001, the Department of Mechanical Engineering of Federal University of Paraná (UFPR), the Federal University of Technology—Paraná (UTFPR) in Apucarana, the UNIESPAÇO program of the Brazilian Space Agency (AEB), and Conselho Nacional de Desenvolvimento Científico e Tecnológico (CNPq), Brazil (Grant No. 308208/2019-6).

Nomenclature

GCI = grid convergence index
p = pressure
p_o = order of accuracy
p_U = equivalent apparent order
Re = Reynolds number
T_c = convergent solution
T_h = numerical solution in the grid h
u = horizontal component of the velocity vector
U_c = estimate of the discretization error of T_c
v = vertical component of the velocity vector
x = horizontal direction
y = vertical direction
μ = viscosity
ρ = density
ψ = stream function

References

[1] Kawaguti, M., 1961, "Numerical Solution of the Navier-Stokes Equations for the Flow in a Two-Dimensional Cavity," J. Phys. Soc. Jpn., **16**(11), pp. 2307–2315.
[2] Burggraf, O. R., 1966, "Analytical and Numerical Studies of the Structure of Steady Separated Flows," J. Fluid Mech., **24**(1), pp. 113–151.
[3] Rubin, S. G., and Khosla, P. K., 1977, "Polynomial Interpolation Methods for Viscous Flow Calculations," J. Comput. Phys., **24**(3), pp. 217–244.
[4] Nallasamy, M., and Prasad, K. K., 1977, "On Cavity Flow at High Reynolds Numbers," J. Fluid Mech., **79**(2), pp. 391–414.
[5] Benjamin, A. S., and Denny, V. E., 1979, "On the Convergence of Numerical Solutions for 2-D Flows in a Cavity at Large Re," J. Comput. Phys., **33**(3), pp. 340–358.
[6] Ghia, U., Ghia, K. N., and Shin, C. T., 1982, "High-Re Solutions for Incompressible Flow Using the Navier-Stokes Equations and a Multigrid Method," J. Comput. Phys., **48**(3), pp. 387–411.
[7] Schreiber, R., and Keller, H. B., 1983, "Driven Cavity Flows by Efficient Numerical Techniques," J. Comput. Phys., **49**(2), pp. 310–333.
[8] Vanka, S. P., 1986, "Block-Implicit Multigrid Solution of Navier-Stokes Equations in Primitive Variables," J. Comput. Phys., **65**(1), pp. 138–158.
[9] Nishida, H., and Satofuka, N., 1992, "Higher-Order Solutions of Square Driven Cavity Flow Using a Variable-Order Multi-Grid Method," Int. J. Numer. Methods Eng., **34**(2), pp. 637–653.
[10] Hou, S., Zou, Q., Chen, S., Doolen, G., and Cogley, A. C., 1995, "Simulation of Cavity Flow by Lattice Boltzmann Method," J. Comput. Phys., **118**(2), pp. 329–347.
[11] Wright, N. G., and Gaskell, P. H., 1995, "An Efficient Multigrid Approach to Solving Highly Recirculating Flows," Comput. Fluids, **24**(1), pp. 63–79.
[12] Barragy, E., and Carey, G. F., 1997, "Stream Function-Vorticity Driven Cavity Solution Using p Finite Elements," Comput. Fluids, **26**(5), pp. 453–468.
[13] Botella, O., and Peyret, R., 1998, "Benchmark Spectral Results on the Lid-Driven Cavity Flow," Comput. Fluids, **27**(4), pp. 421–433.
[14] Erturk, E., Corke, T. C., and Gökçöl, C., 2005, "Numerical Solutions of 2-D Steady Incompressible Driven Cavity Flow at High Reynolds Numbers," Int. J. Numer. Methods Fluids, **48**(7), pp. 747–774.
[15] Bruneau, C. H., and Saad, M., 2006, "The 2D Lid-Driven Cavity Problem Revisited," Comput. Fluids, **35**(3), pp. 326–348.
[16] Marchi, C. H., Suero, R., and Araki, L. K., 2009, "The Lid-Driven Square Cavity Flow: Numerical Solution With a 1024 × 1024 Grid," J. Braz. Soc. Mech. Sci. Eng., **31**(3), pp. 186–198.
[17] Erturk, E., 2009, "Discussions on Driven Cavity Flow," Int. J. Numer. Methods Fluids, **60**(3), pp. 275–294.
[18] Tian, Z., Liang, X., and Yu, P., 2011, "A Higher Order Compact Finite Difference Algorithm for Solving the Incompressible Navier-Stokes Equations," Int. J. Numer. Methods Eng., **88**(6), pp. 511–532.
[19] Khorasanizade, S., and Sousa, J. M. M., 2014, "A Detailed Study of Lid-Driven Cavity Flow at Moderate Reynolds Numbers Using Incompressible SPH," Int. J. Numer. Methods Fluids, **76**(10), pp. 653–668.
[20] Marchi, C. H., Martins, M. A., Novak, L. A., Araki, L. K., Pinto, M. A. V., Gonçalves, S. F. T., Moro, D. F., and Freitas, I. S., 2016, "Polynomial Interpolation With Repeated Richardson Extrapolation to Reduce Discretization Error in CFD," Appl. Math. Modell., **40**(21–22), pp. 8872–8885.
[21] AbdelMigid, T. A., Saqr, K. M., Kotb, M. A., and Aboelfarag, A. A., 2017, "Revisiting the Lid-Driven Cavity Flow Problem: Review and New Steady State Benchmarking Results Using GPU Accelerated Code," Alexandria Eng. J., **56**(1), pp. 123–135.
[22] Yu, Q., Xu, H., Liao, S., and Yang, Z., 2019, "A Novel Homotopy-Wavelet Approach for Solving Stream Function-Vorticity Formulation of Navier-Stokes Equations," Commun. Nonlinear Sci. Numer. Simul., **67**, pp. 124–151.
[23] Romanò, F., and Kuhlmann, H. C., 2017, "Smoothed-Profile Method for Momentum and Heat Transfer in Particulate Flows," Int. J. Numer. Methods Fluids, **83**(6), pp. 485–512.
[24] Albensoeder, S., and Kuhlmann, H. C., 2005, "Accurate Three-Dimensional Lid-Driven Cavity Flow," J. Comput. Phys., **206**(2), pp. 536–558.
[25] Shankar, P. N., and Deshpande, M. D., 2000, "Fluid Mechanics in the Driven Cavity," Annu. Rev. Fluid Mech., **32**(1), pp. 93–136.
[26] Kuhlmann, H. C., and Romanò, F., 2019, "The Lid-Driven Cavity," *Computational Modelling of Bifurcations and Instabilities in Fluid Dynamics*, A. Gelfgat, ed., Springer, Cham, Switzerland, pp. 233–309.
[27] Taylor, G. I., 1962, "On Scraping Viscous Fluid From a Plane Surface," *Miszellangen der Angewandten Mechanik*, M. Shafer, ed., Akademie - Verlag, Berlin, pp. 313–315.
[28] Romanò, F., Türkbay, T., and Kuhlmann, H. C., 2020, "Lagrangian Chaos in Steady Three-Dimensional Lid-Driven Cavity Flow," Chaos, **30**(7), p. 073121.
[29] Stremler, M. A., and Chen, J., 2007, "Generating Topological Chaos in Lid-Driven Cavity Flow," Phys. Fluids, **19**(10), p. 103602.
[30] ASME, 2009, "Standard for Verification and Validation in Computational Fluid Dynamics and Heat Transfer," ASME, New York, Standard No. ASME V&V 20-2009.
[31] Ferziger, J. H., Peric, M., and Street, R. L., 2020, *Computational Methods for Fluid Dynamics*, 4th ed., Springer Nature, Cham, Switzerland.
[32] Khosla, P. K., and Rubin, S. G., 1974, "A Diagonally Dominant Second-Order Accurate Implicit Scheme," Comput. Fluids, **2**(2), pp. 207–209.
[33] Stone, H. L., 1968, "Iterative Solution of Implicit Approximations of Multidimensional Partial Differential Equations," SIAM J. Numer. Anal., **5**(3), pp. 530–558.
[34] Caretto, L. S., Gosman, A. D., Patankar, S. V., and Spalding, D. B., 1972, "Two Calculation Procedures for Steady, Three-Dimensional Flows With Recirculation," Proceedings of the Third International Conference on Numerical Methods in Fluid Dynamics, Paris, France.
[35] Rhie, C. M., and Chow, W. L., 1983, "Numerical Study of the Turbulent Flow Past an Airfoil With Trailing Edge Separation," AIAA J., **21**(11), pp. 1525–1532.
[36] Hackbusch, W., 1985, *Multi-Grid Methods and Applications*, Springer, Berlin.
[37] Roache, P. J., 1994, "Perspective: A Method for Uniform Reporting of Grid Refinement Studies," ASME J. Fluids Eng., **116**(3), pp. 405–413.
[38] Bertoldo, G., and Marchi, C. H., 2017, "Verification and Validation of the Foredrag Coefficient for Supersonic and Hypersonic Flow of Air Over a Cone of Fineness Ratio 3," Appl. Math. Modell., **44**, pp. 409–424.
[39] Marchi, C. H., and Silva, A. F. C., 2002, "Unidimensional Numerical Solution Error Estimation for Convergent Apparent Order," Numer. Heat Transfer, Part B, **42**(2), pp. 167–188.